UKAEA FUS 461

EURATOM/UKAEA Fusion

The nonlinear dynamics of the modulational instability of drift waves and the associated zonal flows

C.N. Lashmore-Davies, D.R. McCarthy* and
A. Thyagaraja

June 2001

EURATOM/UKAEA fusion Association

Culham Science Centre, Abingdon
Oxfordshire, OX14 3DB
United Kingdom
Telephone +44 1235 463357
Facsimile +441235 463435

*Southeastern Louisiana University
Hammond
LA 70402
USA

The nonlinear dynamics of the modulational instability of drift waves and the associated zonal flows

C.N. Lashmore-Davies, D. R. McCarthy* and A. Thyagaraja

EURATOM/UKAEA Fusion Association, Culham Science Centre, Abingdon, OX14 3DB, UK.

*Southeastern Louisiana University

Hammond, LA 70402, USA.

June 14, 2001

Abstract

The linear and nonlinear dynamics of zonal flows and their interactions with drift wave turbulence is considered in the simple but illuminating generalized Charney-Hasegawa-Mima model due to Smolyakov *et. al.*(*A.I. Smolyakov, P.H. Diamond and V.I. Shevchenko, Phys. Plasmas,* **7**, *1349 (2000)*). Two positive definite, exact, integral invariants associated with the full generalized Charney-Hasegawa-Mima system are derived. These invariants are the generalizations of the well-known energy and enstrophy integrals of the original Charney-Hasegawa-Mima equation. Taking the initial pump amplitude as fixed (but small), it is shown that the system experiences a classic 'modulational instability'. This is characterized by the growth of a specified, infinitesimal amplitude zonal flow and side-bands of the pump generated by it beating with the zonal flow. The threshold for this growth is determined and found to be readily satisfied under typical conditions on the pump amplitude and zonal flow perturbation wave number. The pump is then allowed to evolve according to a simple ,'four-wave', nonlinear model. Two positive definite invariants associated with the four-wave evolution are identified. The generalized Charney-Hasegawa-Mima equations are solved numerically. First, the predictions of the analytical 'fixed pump' four-wave model dur-

ing the initial growth phase are verified. The numerical simulations are carried on into the fully nonlinear regime of the system and show explicitly that the exact invariants of the system are indeed conserved to high accuracy over the entire period of simulation (many linear growth times and hundreds of drift wave periods). In contrast it is found that the "four-wave invariants" only remain constant for about three growth times, although this is still long compared to the drift period, thus establishing the time-scale over which the four-wave model retains its validity. The investigation of the long-time behaviour using the simulations demonstrates that the number of effective degrees of freedom of the system as estimated analytically using the exact invariants is in good agreement with that found by the code. Furthermore, the radial structure of the zonal flow can be 'jet-like' or highly oscillatory in space depending upon the values of the density length-scale relative to the system size and initial conditions. It is found that zonal flows can be dramatically reduced if the most unstable zonal flow wave number does not fit into the system. The properties of this relatively simple, two-dimensional, electrostatic, dissipationless model bear a striking resemblance to many features of much more elaborate fluid and kinetic plasma turbulence simulations. As such, the model illustrates the zonal flow/turbulence interaction phenomenon in its most elementary form.

1 Introduction

There is a substantial body of evidence from a variety of magnetic confinement experiments [1]-[3] which shows that sheared radial electric fields and the associated 'zonal $\mathbf{E} \times \mathbf{B}$ flows' play an important role in influencing turbulent transport processes. Such flows are thought to be implicated in the formation and evolution of transport barriers in tokamaks and stellarators[2, 4]. On the theoretical side, a number of researchers[5]-[7] have examined the possibility of suppressing turbulence by radial decorrelation due to strongly sheared $\mathbf{E} \times \mathbf{B}$ flow shear and have contributed a variety of models which exhibit this effect (some of this work is reviewed in [4]-[9]). Interestingly, 'first-principles based' tokamak turbulence simulations of both gyrokinetic[10, 11] and two-fluid[12]-[14] plasma equations of motion also suggest that profile-turbulence interactions are important and lead to strongly sheared radial electric fields. The latter are capable of being generated by the turbulence itself with significant radial fine structure (termed 'corrugations' in [12]), and can, in turn, suppress the turbulence in a complex cyclical process.

Recently, several authors[6, 8] have introduced simplified models of the full plasma equations in order to elucidate the mechanism by which the radial electric fields can be created by turbulence. The simplest model which seems capable of yielding genuine insight is due to Smolyakov *et. al.* [6], where a modified form of the well-known Charney-Hasegawa-Mima equation, involving a nontrivial radial electric field is analysed. In their analysis, these authors used a wave kinetic approach and showed that the 'zonal flow' due to the radial electric field interacts with either a monochromatic 'pump' wave, which is a specified drift wave satisfying the equations of motion or with a turbulent sea of such waves, and induces a modulational (or 'side-band') instability[15, 16]. The instability causes the radial electric field to grow at the expense of the pump wave. The mechanism is laid bare in its simplest form by considering the four-wave interaction of a pump drift wave, a zonal flow and two side-bands of the drift wave generated by the beating of the flow with the pump. In this form, the problem is exactly analogous to the well-known Benjamin-Feir instability in fluid dynamics[15] and to various modulational instabilities in plasmas[17]-[21].

The purpose of the present work is to describe the linear and nonlinear aspects of the modulational instability mechanism for generating radial electric fields associated with zonal flows in this simplest of settings and to point out the interesting and generic features presented by it. We note that the linear instability has been considered in a

special form by Guzdar *et. al.*[8] and recently also in [22]. Our analysis is supported by extensive numerical computations which reveal new features and interesting insights on the problem, not accessible to a wave kinetic approach or to purely linear models of the initial phase. These features bear a striking resemblance to simulations [12] using much more complicated sets of driven, dissipative, global, electromagnetic equations in realistic tokamak conditions. However, the present, simple model appears to contain the essential physics and may offer a more readily understood physical picture of the role and dynamics of zonal flows and their interactions with drift wave turbulence.

The paper is organized as follows. In Section 2 we present a concise account of the governing equations, the assumptions of the model and the exact integrals of motion. The latter are generalizations of the well-known energy and enstrophy integrals of the standard Charney-Hasegawa-Mima equation. We use the invariants to estimate the number of effective degrees of freedom of the system[23, 24]. In Section 3 we derive the simplest form of the modulational instability of a monochromatic pump drift wave due to a zonal flow perturbation, directly modelled on the standard side-band instability theory [15]-[22]. The pump wave amplitude is fixed in this linear description and the dispersion relation leads to the amplitude threshold for the instability. Section 4 is devoted to deriving the full, nonlinear four-wave model, including the evolution of the pump wave and demonstrating the existence of two constants of motion for the four-wave system. Section 5 presents the numerical scheme used to solve the full equations of motion and results obtained from it. Discussion of the significance of the results and conclusions are presented in Section 6.

2 Derivation of the equations of motion and their integral invariants

We use a simple, fluid model to study the nonlinear interaction of drift waves [6, 8, 9]. A slab model of plasma is considered in which the ions are assumed to be cold and the electrons have a uniform temperature, T_e. The equilibrium magnetic field, $\mathbf{B} = B\mathbf{z}$, is assumed to be uniform and oriented along the z-axis. For simplicity we consider a two-dimensional problem in which all quantities are independent of z. The x-direction is analogous to the radial and the y-direction to the poloidal direction in toroidal geometry. All quantities are taken to be periodic in these directions, except for the equilibrium electron number density, $\bar{n}$, which is assumed to vary with x over a length-

scale, $L_n(L_n^{-1} \equiv \frac{1}{\bar{n}(x)}|\frac{d\bar{n}}{dx}|)$. It is convenient to write the full electrostatic potential in the form, $\phi = \bar{\phi} + \tilde{\phi}$, where $\bar{\phi}$ is the y-averaged part (equivalently, it is the $k_y = 0$ Fourier component of the electrostatic potential ϕ) and $\tilde{\phi}$ represents the 'fluctuation' (by definition, a fluctuation must have $k_y \neq 0$). It must be specifically noted however, that *no averaging* with respect to the time is required, nor used. Furthermore, we do not restrict the x variation of $\bar{\phi}(x,t)$ to be 'slow' in any sense. Thus, in principle, $\bar{\phi}(x,t)$ and $\tilde{\phi}(x,y,t)$ can vary with x arbitrarily (subject only to the general limits of validity of fluid models, discussed in the following).

With these conventions, $\mathbf{V}_0 = cz \times \nabla\bar{\phi}/B$ is the y-averaged $\mathbf{E} \times \mathbf{B}$ drift (this will be consistently referred to in this paper as the 'zonal flow'), whilst $\tilde{\mathbf{V}}_E = cz \times \nabla\tilde{\phi}/B$ represents the fluctuating $\mathbf{E} \times \mathbf{B}$ drift, and $\mathbf{V}_d = V_d\mathbf{y}$ is the diamagnetic drift. The nonlinear behaviour of the electrostatic potential is described by the following well-known equation[6, 9]:

$$(\frac{\partial}{\partial t} + \mathbf{V}_0.\nabla + \mathbf{V}_d.\nabla)\frac{e\tilde{\phi}}{T_e} - (\frac{\partial}{\partial t} + \mathbf{V}_0.\nabla + \tilde{\mathbf{V}}_E.\nabla)\rho_s^2\nabla_\perp^2\frac{e\phi}{T_e} = 0, \qquad (1)$$

where, $\rho_s = c_s/\Omega_{ci}$, and $c_s = (2T_e/m_i)^{1/2}$, $\Omega_{ci} = eB/m_ic$. We note that the fluid model is nominally valid in the present 'cold-ion' approximation even for high perpendicular wave numbers, $k_\perp$ such that $(k_\perp\rho_s \geq 1)$. However, we consider initial conditions for which all perturbations satisfy the 'long wavelength ordering', $k_\perp\rho_s \ll 1$, noting that typical experimental values of this parameter lie in the range, $0.1 - 0.5$. The integral invariants which we derive guarantee that the initial wavenumber ordering assumed is preserved for all subsequent times. We shall also find that the modulational instability is limited to relatively small wavenumbers in general.

We take the system dimensions in the x, y directions to be given respectively by a and L_y. Usually, these lengths are of the same order, and it is convenient in calculations to set them equal. The averaged electrostatic potential, $\bar{\phi}$, is related to the total potential, ϕ, as follows:

$$\begin{aligned} \bar{\phi} &= (1/L_y)\int_0^{L_y}\phi dy \\ &= <\phi>_y . \end{aligned} \qquad (2)$$

The following standard normalizations are used: $\hat{\rho} \equiv \rho_s/a, \phi \rightarrow e\phi/T_e, x \rightarrow x/a, y \rightarrow y/L_y, t \rightarrow (\rho_s c_s/a^2)t, \mathbf{v}_{E\times B} = \frac{\rho_s c_s}{a}\mathbf{z} \times \nabla\phi, V_d = \alpha\rho_s c_s/a$, where $\alpha \equiv a/L_n$ is a nondimensional measure of the equilibrium density gradient in the x-direction.

It is then easy to cast Eq.(1) into a pair of dimensionless nonlinear, coupled equations for $\bar{\phi}(x,t)$ and $\hat{f} \equiv (1-\hat{\rho}^2\nabla_\perp^2)\tilde{\phi}$:

$$\frac{\partial \bar{\phi}_{xx}}{\partial t} + < (\mathbf{z} \times \nabla\tilde{\phi}).\nabla\nabla_\perp^2\tilde{\phi} >_y \;=\; 0. \tag{3}$$

$$\frac{\partial \hat{f}}{\partial t} + \mathbf{V}.\nabla\hat{f} + \hat{\rho}^2 < (\mathbf{z} \times \nabla\tilde{\phi}).\nabla\nabla_\perp^2\tilde{\phi} >_y + \hat{\rho}^2\left[\alpha\frac{\partial\nabla_\perp^2\tilde{\phi}}{\partial y} + \frac{\partial\tilde{\phi}}{\partial y}\frac{\partial\bar{\phi}_{xx}}{\partial x}\right] \;=\; 0, \tag{4}$$

where, $\mathbf{V} \equiv \tilde{\mathbf{V}}_E + \mathbf{V}_0 + \mathbf{V}_d$. Note that $\nabla.\mathbf{V} = 0$.

We now derive two important integral invariants associated with this system. They generalize well-known results for the original Charney-Hasegawa-Mima equation, and throw light on the nonlinear evolution properties of the solutions to the equations of motion given above.

The preceding equations can be rewritten as follows. We may multiply Eq.(3) by $-\hat{\rho}^2$ and use the following simple relations:

$$\begin{aligned} (\mathbf{z} \times \nabla\tilde{\phi}).\nabla\nabla_\perp^2\tilde{\phi} &= \mathbf{z}.(\nabla\tilde{\phi} \times \nabla\nabla_\perp^2\tilde{\phi}). \\ &= \frac{\partial(\tilde{\phi}, \nabla_\perp^2\tilde{\phi})}{\partial(x,y)} \\ \frac{\partial(\tilde{\phi}, \tilde{\phi})}{\partial(x,y)} &= 0. \end{aligned} \tag{5}$$

We introduce the 'mean vorticity', F:

$$F(x,t) \;=\; -\hat{\rho}^2\bar{\phi}_{xx}. \tag{6}$$

It then follows (from Eq.(3)) that F satisfies,

$$\frac{\partial F}{\partial t} + < \frac{\partial(\tilde{\phi}, \hat{f})}{\partial(x,y)} >_y \;=\; 0,$$

i.e.,

$$\frac{\partial F}{\partial t} + < \frac{\partial}{\partial x}(-\frac{\partial\tilde{\phi}}{\partial y}\hat{f}) + \frac{\partial}{\partial y}(\frac{\partial\tilde{\phi}}{\partial x}\hat{f}) >_y \;=\; 0. \tag{7}$$

Averaging over y, using the periodicity, the equation becomes (here, R is the 'Reynolds stress due to the fluctuations which drive the zonal flows),

$$\frac{\partial F}{\partial t} + \frac{\partial R}{\partial x} = 0. \tag{8}$$

$$R(x,t) = -\int_0^1 \frac{\partial \tilde{\phi}}{\partial y} \hat{f} dy. \tag{9}$$

The expression for R can be usefully simplified by substituting for $\hat{f}$:

$$\begin{aligned} R &= \hat{\rho}^2 \int_0^1 \frac{\partial \tilde{\phi}}{\partial y} \left[\frac{\partial^2 \tilde{\phi}}{\partial x^2} + \frac{\partial^2 \tilde{\phi}}{\partial y^2} \right] dy \\ &= \frac{\partial}{\partial x} \left[\hat{\rho}^2 \int_0^1 \frac{\partial \tilde{\phi}}{\partial y} \frac{\partial \tilde{\phi}}{\partial x} dy \right]. \end{aligned} \tag{10}$$

The last equation may be integrated with respect to x over the domain using periodic boundary conditions (in x) and gives the exact relation of subsequent importance,

$$\int_0^1 R dx = 0. \tag{11}$$

Next we transform Eq.(4) introducing the definitions introduced above for R, F as follows:

$$\frac{\partial \hat{f}}{\partial t} + \mathbf{V}.\nabla \hat{f} - \frac{\partial R}{\partial x} - \alpha \frac{\partial \hat{f}}{\partial y} + \alpha \frac{\partial \tilde{\phi}}{\partial y} - \frac{\partial \tilde{\phi}}{\partial y} \frac{\partial F}{\partial x} = 0.$$

Using the definitions of $\mathbf{V}, \mathbf{V}_0, \mathbf{V}_d$ and $\hat{f}$, we may put this equation in the form:

$$\frac{\partial \hat{f}}{\partial t} + \mathbf{V}_0.\nabla \hat{f} + \tilde{\mathbf{V}}_E.\nabla \hat{f} - \frac{\partial R}{\partial x} + \alpha \frac{\partial \tilde{\phi}}{\partial y} - \frac{\partial \tilde{\phi}}{\partial y} \frac{\partial F}{\partial x} = 0. \tag{12}$$

Noting that, $\mathbf{V}_0.\nabla F \equiv 0$, Eq.(8) and the relation, $\tilde{\mathbf{V}}_E.\nabla F = -\frac{\partial \tilde{\phi}}{\partial y} \frac{\partial F}{\partial x}$, the above equation for the time evolution of $\hat{f}$ may be written in the remarkably simple form,

$$\frac{\partial (\hat{f} + F)}{\partial t} + \mathbf{V}_0.\nabla (\hat{f} + F) + \tilde{\mathbf{V}}_E.\nabla (\hat{f} + F) + \alpha \frac{\partial \tilde{\phi}}{\partial y} = 0. \tag{13}$$

We now derive exact invariant integrals for the system. Integrating Eq.(12) over y, we obtain the 'trivial' invariant,

$$\frac{\partial}{\partial t} \int_0^1 \hat{f} dy = 0. \tag{14}$$

This follows from periodicity in y and the definition of R. Fluctuations are defined by the condition, $\int_0^1 \hat{f} dy = 0$. The invariant guarantees the consistency of this definition

for all times, provided it is applied at $t = 0$. It is easily verified that this also implies the consistency of $\int_0^1 \tilde{\phi} dy = 0$ for all time. Turning to Eq.(13), we multiply by the function $\hat{f} + F$ and integrate over the whole (periodic) x, y domain. The advective terms may all be disposed off by suitable applications of the divergence theorem, leaving us with,

$$\begin{aligned} \frac{d}{dt}\int\int(\hat{f}+F)^2 dxdy + 2\alpha\int\int(\hat{f}+F)\frac{\partial\tilde{\phi}}{\partial y}dxdy &= 0, \\ \frac{d}{dt}\int\int(\hat{f}+F)^2 dxdy &= -2\alpha\int\int\hat{f}\frac{\partial\tilde{\phi}}{\partial y}dxdy \\ &= 0. \end{aligned} \tag{15}$$

by virtue of periodicity, independence of F on y and Eq.(11). Since it follows from Eq.(14) that $\int\int F\hat{f}dxdy = 0$ for all time, we obtain the invariance of the positive definite integral,

$$I \equiv \int\int(\hat{f}^2 + F^2)dxdy, \tag{16}$$

where I represents the total (ie, integrated) enstrophy of the system. It clearly depends on the second-order derivatives of the potential. Furthermore, this invariant demonstrates that no motion of this system can be *unbounded* (i.e., the system is Lagrange stable in the sense of [23, 24]) even though linear stability may fail to hold; all linearly unstable modes *must* be nonlinearly saturated.

A second invariant, quadratic in the potentials, can be derived as follows: Eq.(12) can be expanded out (using the definitions):

$$\frac{\partial\tilde{\phi}}{\partial t} - \hat{\rho}^2\frac{\partial\nabla^2\tilde{\phi}}{\partial t} + \frac{\partial\bar{\phi}}{\partial x}\frac{\partial\hat{f}}{\partial y} = -\frac{\partial(\tilde{\phi},\hat{f})}{\partial(x,y)} + \frac{\partial R}{\partial x} - \alpha\frac{\partial\tilde{\phi}}{\partial y} + \frac{\partial\tilde{\phi}}{\partial y}\frac{\partial F}{\partial x}. \tag{17}$$

Multiplying this equation by $\tilde{\phi}$ and integrating over the whole x, y domain, we see that the terms on the right vanish by virtue of the periodicity of $\tilde{\phi}$ in y and Eq.(14). The first two terms on the left hand side are readily transformed by the judicious use of the divergence theorem, and take the form, $\frac{d}{dt}\int\int\frac{1}{2}\left[\bar{\phi}^2 + \hat{\rho}^2\tilde{\phi}_x^2 + \hat{\rho}^2\tilde{\phi}_y^2\right]dxdy$. The third term on the left is transformed as follows:

$$\begin{aligned} \int\int\tilde{\phi}\frac{\partial\bar{\phi}}{\partial x}\frac{\partial\hat{f}}{\partial y}dxdy &= \int\frac{\partial\bar{\phi}}{\partial x}dx\int(-\hat{f}\frac{\partial\tilde{\phi}}{\partial y})dy \\ &= \int\frac{\partial\bar{\phi}}{\partial x}Rdx \\ &= -\int\frac{\partial R}{\partial x}\bar{\phi}dx \end{aligned}$$

$$
\begin{aligned}
&= \int \bar{\phi} \frac{\partial F}{\partial t} dx \\
&= -\hat{\rho}^2 \int \bar{\phi} \bar{\phi}_{xxt} dx \\
&= \frac{d}{dt} \int \int \frac{1}{2} \hat{\rho}^2 \bar{\phi}_x^2 dx dy, \qquad (18)
\end{aligned}
$$

where we have made use of Eqs.(6,8) and (9).

These manipulations lead to the establishment of a second, positive definite quadratic integral invariant,

$$
\frac{d}{dt} \int \int \left[\tilde{\phi}^2 + \hat{\rho}^2 (\tilde{\phi}_x^2 + \tilde{\phi}_y^2 + \bar{\phi}_x^2) \right] dx dy \;=\; 0. \qquad (19)
$$

Thus, denoting this 'energy integral' by J, the second constant of motion for the system is:

$$
J \;=\; \int \int \left[\tilde{\phi}^2 + \hat{\rho}^2 (\tilde{\phi}_x^2 + \tilde{\phi}_y^2 + \bar{\phi}_x^2) \right] dx dy. \qquad (20)
$$

Unlike the enstrophy integral I, the energy integral J only involves the first order partial derivatives of the potential. It is entirely reasonable to expect this system to have *effectively a finite number of degrees of freedom*[23, 24]. In order to estimate this number, we consider the invariant, $Q = (I - J)/\hat{\rho}^2 J$. Evidently, Q does not depend on the normalization of the fluctuation level, $\tilde{\phi}$. The numerator can be simplified and becomes, after suitable integrations by parts,

$$
I - J \;=\; \hat{\rho}^2 \int \int \left[(\tilde{\phi}_x^2 + \tilde{\phi}_y^2 - \bar{\phi}_x^2) + \hat{\rho}^2 (\nabla_\perp^2 \tilde{\phi})^2 + \hat{\rho}^2 \bar{\phi}_{xx}^2 \right] dx dy. \qquad (21)
$$

We note firstly that $\bar{\phi}$ is *driven* by the fluctuations in this model, and is hence formally $O(\tilde{\phi}^2)$. For this reason, $I > J$ in all practical cases, since $\tilde{\phi} \ll 1$. Utilizing our wavenumber ordering, we find that (since the terms involving $\hat{\rho}$ are small compared with the others in this ordering), $I - J \simeq \hat{\rho}^2 \int \int \left[\tilde{\phi}_x^2 + \tilde{\phi}_y^2 \right] dx dy$, and by the same token, $J \simeq \int \int \tilde{\phi}^2 dx dy$. It follows that,

$$
\begin{aligned}
Q &= (I - J)/J\hat{\rho}^2 \\
&\simeq \frac{\int \int \left[\tilde{\phi}_x^2 + \tilde{\phi}_y^2 \right] dx dy}{\int \int \tilde{\phi}^2 dx dy}. \qquad (22)
\end{aligned}
$$

According to [23, 24], the *number of effective degrees of freedom*, N_{eff} is given by,

$$
N_{\text{eff}} \;=\; Q^{1/2}/2\pi. \qquad (23)
$$

It is important to observe that these invariants are exact consequences of the nonlinear equations of motion. They can also be readily derived for homogeneous boundary conditions in x (periodic in y). The structure of the system suggests that there are no other *quadratic* invariants, although this fact and the nonexistence of other, nontrivial, independent invariant integrals has not been conclusively established. Note that the existence of these positive definite integral invariants does *not* preclude *Lyapunov instability* or 'sensitive dependence' of solutions to the initial value problem on the initial data. Thus the motion, although bounded and hence Lagrange stable and recurrent, could be 'chaotic' (i.e., possess nontrivial frequency power spectra with both 'coherent/quasi-periodic ' and 'broad-band/turbulent' components).

3 Modulational instability of drift waves in a slab

In this section we consider the relationship of the modulational instability of a monochromatic drift wave to the generation of a zonal flow. We have already identified the y-averaged potential $\bar{\phi}(x,t)$ with a zonal flow $\mathbf{V}_0$. Notice that the time evolution of the zonal flow (Eq.(3)) is due entirely to the nonlinear coupling of drift wave fluctuations. The nonlinear dynamics of the drift wave fluctuations in the presence of zonal flow is described by Eq.(4). In general, a turbulent spectrum of drift wave fluctuations will be present in a plasma. Here, we simplify the problem by assuming that there is just a single, finite amplitude, monochromatic drift wave present initially, whose frequency and wave number are given by, $(\omega_0, \mathbf{k}_0)$ where, $\mathbf{k}_0 = (k_x, k_y, 0)$ and,

$$\omega_0 = \frac{\alpha k_y}{1+\hat{\rho}^2 k_0^2}, \tag{24}$$

with,

$$k_0^2 = k_x^2 + k_y^2. \tag{25}$$

Now assume the presence of a zonal flow fluctuation $(\omega, \mathbf{q})$ with wave number $\mathbf{q} = (q, 0, 0)$, which varies on a time-scale much longer than ω_0^{-1} and is to be determined. The zonal flow fluctuation can then beat with the finite amplitude pump wave to generate drift wave sidebands with wave numbers, $\mathbf{k}_\pm = \mathbf{k}_0 \pm \mathbf{q} = (k_x \pm q, k_y, 0)$. The sidebands, in turn, can beat with the pump wave to reinforce the zonal flow fluctuation, thus closing the feedback loop. This is the mechanism underlying modulational instabilities which have been studied in the fields of laser plasma interactions, magnetized plasmas and fluids ([15]-[21]).

Let us now obtain the equations for the two sideband amplitudes from Eq.(4). The pump wave is assumed to have the following form:

$$\tilde{\phi}_0 = A_0(t)\exp(ik_x x + ik_y y - i\omega_0 t) + c.c., \tag{26}$$

and the sidebands,

$$\tilde{\phi}_\pm = A_\pm(t)\exp(i(k_x \pm q)x + ik_y y - i\omega_\pm t) + c.c. \tag{27}$$

In this expression, the unperturbed drift wave frequencies, $\omega_\pm$, are given by,

$$\omega_\pm = \frac{\alpha k_y}{1+\hat{\rho}^2 k_\pm^2}, \tag{28}$$

where $k_\pm^2 = (k_x \pm q)^2 + k_y^2$. The zonal flow perturbation is assumed to be of the form,

$$\mathrm{V}_0 = \hat{\rho}c_s \mathrm{y}\left[iqB(t)\exp(iqx) + c.c\right], \tag{29}$$

where, q is the dimensionless 'radial' wave number, and $B(t)$, the amplitude. The equations for the side band amplitudes $A_\pm$ can be obtained by substituting Eqs.(26-29) into Eq.(4) and keeping only the terms which satisfy perfect wave number matching. The equations are:

$$\frac{dA_+}{dt} = \Omega_0 \Lambda_+ A_0 B \exp(i\delta_+ t), \tag{30}$$

$$\frac{dA_-}{dt} = -\Omega_0 \Lambda_- A_0 B^* \exp(i\delta_- t), \tag{31}$$

where,

$$\delta_\pm = \omega_\pm - \omega_0. \tag{32}$$

The interaction coefficients, $\Omega_0, \Lambda_\pm$, are given by,

$$\Omega_0 = qk_y, \tag{33}$$

$$\Lambda_\pm = \frac{1+\hat{\rho}^2(k_0^2 - q^2)}{1+\hat{\rho}^2 k_\pm^2}, \tag{34}$$

and we emphasize that wave numbers and amplitudes appearing in Eqs.(31-32) are normalized as defined below Eq.(2).

The equation for B can be obtained by substituting Eqs.(26-29) into Eq.(3) and again using perfect wave number matching. We thus obtain,

$$\frac{dB}{dt} = \Omega_0\left[\mu_+ A_+ A_0^* \exp(-i\delta_+ t) - \mu_- A_-^* A_0 \exp(i\delta_- t)\right], \tag{35}$$

where,

$$\mu_{\pm} = \frac{(k_{\pm}^2 - k_0^2)}{q^2}. \tag{36}$$

The set of equations (30), (31) and (35) allows us to obtain the conditions for modulational instability of a finite amplitude drift wave, $\tilde{\phi}_0$. If the nonlinear coupling terms in Eqs.(30-35), are neglected, then $A_{\pm}$ represent infinitesimal drift waves oscillating at their natural frequencies, $\omega_{\pm}$. It is helpful to introduce modified amplitude functions by the relations,

$$A_{\pm}(t) = a_{\pm}(t)\exp(i\delta_{\pm}t). \tag{37}$$

The coupled equations, (30), (31) and (35) then take the form,

$$\frac{da_+}{dt} + i\delta_+ a_+ = \Omega_0 \Lambda_+ A_0 B, \tag{38}$$

$$\frac{da_-}{dt} + i\delta_- a_- = -\Omega_0 \Lambda_- A_0 B^*, \tag{39}$$

$$\frac{dB}{dt} = \Omega_0(\mu_+ a_+ A_0^* - \mu_- a_-^* A_0). \tag{40}$$

The coupled equations (38-40) describe the nonlinear interaction of a finite amplitude drift wave to two other, sideband drift waves through a zonal flow perturbation with wave number $\mathbf{q} = (q, 0, 0)$. This coupling is less restrictive than the resonant decay of a drift wave into two other drift waves and there is no constraint on q. Since the 'pump amplitude' A_0 has been assumed large compared with the sideband amplitudes, it can be assumed to remain constant during the initial phase of the interaction. Hence Eqs.(38-40) are linearized, and since the coefficients are all independent of the time, we may solve the system by assuming that a_+, a_-^* and B all vary as $\exp(-i\omega t)$. Substituting this variation into Eqs.(38-40), we obtain the dispersion relation:

$$-\omega = \Omega_0^2 |A_0|^2 \left[\frac{\mu_+ \Lambda_+}{\omega - \delta_+} + \frac{\mu_- \Lambda_-}{\omega + \delta_-}\right]. \tag{41}$$

Although formally this is a cubic, we can show easily that $\omega = 0$ is a root (a marginal mode). To see this, we set $\omega = 0$ in both sides of Eq.(41). Consistency demands that the terms on the right must also vanish. This holds if and only if the following identity applies:

$$\frac{\mu_+ \Lambda_+}{\delta_+} = \frac{\mu_- \Lambda_-}{\delta_-}. \tag{42}$$

Substituting Eqs.(32), (34) and (36) in Eq.(42), we see that,

$$\begin{aligned}\frac{\mu_+\Lambda_+}{\delta_+} &= \frac{(k_+^2-k_0^2)}{q^2}\left(\frac{1+\hat{\rho}^2(k_0^2-q^2)}{1+\hat{\rho}^2k_+^2}\right)\left(\frac{1}{\omega_+-\omega_0}\right)\\ &= -\frac{1+\hat{\rho}^2(k_0^2-q^2)}{\omega_0\hat{\rho}^2q^2}\\ &= -F_0(k_0,q)\\ &= \frac{\mu_-\Lambda_-}{\delta_-},\end{aligned}$$

where, $F_0(k_0,q)$ is the function defined by ,

$$F_0(k_0,q) = \frac{1+\hat{\rho}^2(k_0^2-q^2)}{\omega_0\hat{\rho}^2q^2}. \tag{43}$$

These considerations reduce the dispersion relation to the quadratic:

$$\omega^2+\omega(\delta_--\delta_+)-\delta_+\delta_--\Omega_0^2|A_0|^2F_0(k_0,q)(\delta_++\delta_-) = 0, \tag{44}$$

where we have made use of Eq.(42). The solution of this equation is,

$$\omega = \frac{1}{2}\left\{\delta_+-\delta_-\pm\left[(\delta_++\delta_-)^2+4\Omega_0^2|A_0|^2F_0(k_0,q)(\delta_++\delta_-)\right]^{1/2}\right\}. \tag{45}$$

With the aid of Eqs.(24) and (32) we find that,

$$\delta_++\delta_- = -\frac{2\omega_0\hat{\rho}^2q^2\left[1+\hat{\rho}^2(k_y^2+q^2-3k_x^2)\right]}{(1+\hat{\rho}^2k_+^2)(1+\hat{\rho}^2k_-^2)}, \tag{46}$$

$$\delta_+-\delta_- = -\frac{4\omega_0k_x\hat{\rho}^2q(1+\hat{\rho}^2k_0^2)}{(1+\hat{\rho}^2k_+^2)(1+\hat{\rho}^2k_-^2)}. \tag{47}$$

These expressions may be simplified in the long wavelength ordering: $\hat{\rho}^2k_0^2 \ll 1, \hat{\rho}^2k_\pm^2 \ll 1, \hat{\rho}^2q^2 \ll 1$. The solution to the dispersion relation can then be approximated by the following form:

$$\omega \simeq -2\omega_0k_xq\hat{\rho}^2 \pm \omega_0\hat{\rho}^2q^2\left[1-\frac{2k_y^2|A_0|^2}{\omega_0^2\hat{\rho}^4q^2}\right]^{1/2}. \tag{48}$$

Hence, the finite amplitude drift wave will be modulationally unstable if,

$$\begin{aligned}|A_0|^2 &> \frac{\omega_0^2q^2\hat{\rho}^4}{2k_y^2}\\ &> (\rho_sq)^2\frac{V_d^2}{2c_s^2},\end{aligned} \tag{49}$$

where we revert to dimensional variables in the right hand side of the last inequality for clarity. Clearly the threshold is very low since $V_d^2 \ll c_s^2$, and $(\rho_s q)^2 \ll 1$. We note that the threshold amplitude is proportional to the 'drift Mach number' defined by, $M_d = |V_d|/c_s$ and to $|q|$. Using Eq.(48), the growth rate can be written as:

$$\gamma^2 \approx k_y^2 \alpha^2 q^2 (\frac{2A_0^2}{\alpha^2 \hat{\rho}^2} - q^2 \hat{\rho}^2). \tag{50}$$

Since γ^2 is parabolic in q^2, it is straightforward to show that the maximum growth rate occurs for

$$q_{max} \approx \frac{A_0}{\alpha \hat{\rho}^2}, \tag{51}$$

The threshold condition also implies that for modulational instability, q (the dimensional radial wave number of the zonal flow) must be in the unstable band given by,

$$0 < \rho_s q < \sqrt{2}(c_s/V_d)|A_0|. \tag{52}$$

Furthermore, the wave number corresponding to maximum growth is,

$$(\rho_s q)_{\max} = (c_s/V_d)|A_0|. \tag{53}$$

While the threshold amplitude is higher for larger q^2, the growth rate is also larger.This can be seen by the following expression for the growth-rate γ, well above the threshold:

$$\gamma \approx k_y q \sqrt{2}|A_0| \tag{54}$$

The instability results in growing sideband drift waves with radial wave numbers $k_x \pm q$ and a growing zonal flow perturbation with a radial wavenumber q. The $k_x + q$ and $k_x - q$ sidebands (i.e., $\tilde{\phi}_\pm$) oscillate at frequencies $\omega_0 \pm \omega_r$ respectively whilst the zonal flow oscillates at ω_r where, $\omega_r \simeq -2\omega_0 k_x q \rho_s^2$.

It is interesting to consider the 'typical' wave number ordering, $q^2 \ll k_x^2 < k_0^2$. Evidently, $F_0(k_0, q) > 0$, in all such cases. For this ordering, we may Taylor expand $\omega_\pm(\mathbf{k}, \mathbf{q})$ in powers of q:

$$\omega_\pm(\mathbf{k}, q) = \omega_0 + \frac{\partial \omega_0}{\partial k_x} q + \frac{\partial^2 \omega_0}{\partial k_x^2} \frac{q^2}{2!} + .. \tag{55}$$

Denoting by $V_{gx} \equiv \frac{\partial \omega_0}{\partial k_x}$, the group velocity (in our dimensionless units) in the $x-$direction, we see that,

$$\begin{aligned} \delta_+ + \delta_- &= \omega_+ + \omega_- - 2\omega_0 \\ &= q^2 \frac{\partial^2 \omega_0}{\partial k_x^2} \\ &= q^2 \frac{\partial V_{gx}}{\partial k_x}. \end{aligned} \tag{56}$$

In consequence, the threshold condition can be rewritten (taking account of the wave number orderings),

$$|A_0|^2 \;>\; \left\{\frac{-q^2}{\omega_0}\frac{\partial V_{gx}}{\partial k_x}\right\}\left(\frac{V_d^2}{4c_s^2}\right). \tag{57}$$

It is clear that a necessary condition for instability is that $\frac{1}{\omega_0}\frac{\partial V_{gx}}{\partial k_x} < 0$. This is always satisfied, as can be verified from Eq.(24). These results are in agreement with those of Refs.[6, 8, 22] for the appropriate orderings.

4 Nonlinear evolution and invariants in the reduced four-wave model

In the previous section we have described the modulational instability of a finite amplitude drift wave due to nonlinear coupling to a single pair of sideband drift waves and a low frequency zonal flow perturbation. The properties of the instability were obtained by assuming that the amplitude of the finite amplitude drift wave (the pump wave) was much larger than the side band amplitudes so that the reaction of the other waves on the pump wave was neglected and the pump itself was assumed to remain constant. This enabled us to linearize the coupled equations and the resulting modulational instability represents the initial phase of the development of this nonlinear interaction.

In this section we analyze the nonlinear evolution of this four-wave interaction in which the pump wave is treated on the same footing as the sideband drift waves. In order to do this we must obtain an equation for the pump wave. This can be derived using Eqs.(4,26) in a manner similar to that used to obtain the equations for the side bands. Thus retaining only terms which satisfy perfect wave number matching, we obtain an equation for the pump wave amplitude $A_0(t)$, introduced in Eq.(26). The equation is,

$$\frac{dA_0}{dt} \;=\; -\Omega_0(\nu_+ a_+ B^* - \nu_- a_- B), \tag{58}$$

where, $\nu_\pm$ are defined as follows:

$$\nu_\pm \;=\; \frac{1+\hat{\rho}^2(k_\pm^2 - q^2)}{1+\hat{\rho}^2 k_0^2}. \tag{59}$$

The nonlinear evolution of the modulational instability for a given perturbed wave number q (say that corresponding to the maximum growth rate) is described by Eqs.(38)-(40) and Eq.(58). It should be understood that these equations, together with their conjugate complex ones, govern the dynamics of the four *complex amplitudes*, $a_\pm, A_0, B$. We note that all the parameters appearing in the above equations are *real*. It is not evident from the existence of the exact integral invariants that the four-wave equations must have any invariants of their own. However, we show now that two such invariants do indeed exist, and give a derivation of them directly, without reference to I, J derived earlier.

From the above equations and their complex conjugates, we readily obtain the following equations governing the real wave 'intensities':

$$\begin{aligned}
\frac{d|A_0|^2}{dt} &= -\Omega_0(\nu_+ A_0^* a_+ B^* - \nu_- A_0^* a_- B) \\
&\quad -\Omega_0(\nu_+ A_0 a_+^* B - \nu_- A_0 a_-^* B^*), && (60)\\
\frac{d|B|^2}{dt} &= \Omega_0(\mu_+ A_0^* a_+ B^* - \mu_- A_0 a_-^* B^*) \\
&\quad +\Omega_0(\mu_+ A_0 a_+^* B - \mu_- A_0^* a_- B), && (61)\\
\frac{d|a_+|^2}{dt} &= \Omega_0 \Lambda_+ A_0 a_+^* B + \Omega_0 \Lambda_+ A_0^* a_+ B^*, && (62)\\
\frac{d|a_-|^2}{dt} &= -\Omega_0 \Lambda_- A_0 a_-^* B^* - \Omega_0 \Lambda_- A_0^* a_- B. && (63)
\end{aligned}$$

To find invariants, we multiply Eqs.(61-63) by the undetermined, real, constant (in time) multipliers, λ_B, λ_+ and λ_-, respectively and add the four equations to obtain:

$$\begin{aligned}
\frac{1}{\Omega_0}\frac{d}{dt}(|A_0|^2 + \lambda_B|B|^2 + \lambda_+|a_+|^2 + \lambda_-|a_-|^2) &= A_0^* a_+ B^* [-\nu_+ + \lambda_B \mu_+ + \lambda_+ \Lambda_+] \\
&\quad + A_0 a_-^* B^* [\nu_- - \lambda_B \mu_- - \lambda_- \Lambda_-] \\
&\quad + c.c. && (64)
\end{aligned}$$

Evidently we can make the right hand side of Eq.(64) vanish by choosing the multipliers to satisfy the relations,

$$\begin{aligned}
\nu_+ &= \lambda_B \mu_+ + \lambda_+ \Lambda_+, && (65)\\
\nu_- &= \lambda_B \mu_- + \lambda_- \Lambda_-. && (66)
\end{aligned}$$

These relations can be solved for $\lambda_\pm$ in terms of λ_B and the other parameters of the problem:

$$\lambda_\pm = (\nu_\pm - \lambda_B \mu_\pm)/\Lambda_\pm. \qquad (67)$$

This result implies that the following quadratic function $W(A_0, B, a_\pm)$ of the amplitudes, containing the parameters appearing in the equations of motion and the 'free parameter' λ_B, is a constant of the motion of the system of nonlinear equations, Eqs.(38-40), (58), for *arbitrary* values of λ_B:

$$\begin{aligned} W \equiv & \left[|A_0|^2 + (\nu_+/\Lambda_+)|a_+|^2 + (\nu_-/\Lambda_-)|a_-|^2\right] \\ & +\lambda_B \left[|B|^2 - (\mu_+/\Lambda_+)|a_+|^2 - (\mu_-/\Lambda_-)|a_-|^2\right]. \end{aligned} \tag{68}$$

It is clear that we have derived in this way, the only two *functionally independent* constants of the motion of the system which are quadratic in the amplitudes. These are respectively, the term independent of λ_B and the coefficient of λ_B in Eq.(68) above:

$$I_0 \equiv |A_0|^2 + (\nu_+/\Lambda_+)|a_+|^2 + (\nu_-/\Lambda_-)|a_-|^2, \tag{69}$$

$$I_B \equiv |B|^2 - (\mu_+/\Lambda_+)|a_+|^2 - (\mu_-/\Lambda_-)|a_-|^2. \tag{70}$$

It is obvious that an arbitrary function of these invariants is also an invariant. Thus, W itself is a *linear* function of I_0, I_B, and is therefore not independent of these. It is conjectured but not proven that for generic values of the parameters $\Lambda_\pm, \mu_\pm, \nu_\pm$ appearing in the governing equations, the system possesses no other invariants functionally independent of I_0, I_B. Observe that the four-wave system governed by Eqs.(38-40) and Eq.(58) is represented by four complex amplitudes (equivalent to eight real functions of time). The existence of two real constants of the motion reduce the number of independent real functions required to represent the system from eight to six. It is also of interest to observe that I_0 is an invariant solely involving the 'pump' wave and its two side-bands, whilst I_B involves only the 'zonal flow' and the two side-bands. The pump and the zonal flow are obviously coupled to each other via the side-bands.

5 Numerical simulation results

In order to develop a fuller understanding of the nonlinear behavior of this system, we solve Eqs. (3) and (4) using a two dimensional (2-D) finite difference code. This code employs a second order accurate, explicit time stepping procedure. All spatial derivatives are evaluated using a five point finite difference scheme that is accurate to Δ^2, where Δ is the grid spacing. The convective derivatives are stabilized with a velocity dependent hyperviscosity [25]. This is similar to a typical upwind differencing technique. However, the hyperviscosity is also evaluated using a five point differencing

scheme, resulting in the overall method having a high degeee of accuracy and stability. The time stepping procedure uses an explicit trapezoidal leapfrog scheme, which is accurate to $(\Delta t)^2$, where Δt is the time step. The details of these numerical algorithms are discussed in Ref. [25]. The two variables evolved were $\hat{f} = (1 - \hat{\rho}^2\nabla_\perp^2)\bar{\phi}$ and $\bar{\phi}_{xx}$ which were then inverted using Fourier transforms to find $\bar{\phi}$ and $\bar{\phi}$ respectively. We have checked the basic schemes used in the code by solving the equations of motion separately, when the nonlinear coupling terms are specified functions, effectively linearizing the equations.

We write the equations Eqs.(3,4) in the following form,

$$\frac{\partial \bar{\phi}_{xx}}{\partial t} + < \hat{\Sigma}(x,y) >_y = 0, \tag{71}$$

$$\frac{\partial \hat{f}}{\partial t} + \nabla \cdot (\mathbf{V}_0 \hat{f}) - \hat{\rho}^2[\hat{\Sigma}(x,y) - < \hat{\Sigma}(x,y) >_y] + \alpha \frac{\partial \bar{\phi}}{\partial y} + \hat{\rho}^2 \frac{\partial \bar{\phi}}{\partial y}\frac{\partial \bar{\phi}_{xx}}{\partial x} = 0, \tag{72}$$

where we have used, $\nabla.\mathbf{V}_0 = 0$, the expression for $\tilde{\mathbf{V}}_E$ and the definition, $\hat{\Sigma}(x,y) \equiv \hat{z} \times \nabla\tilde{\phi} \cdot \nabla\nabla_\perp^2\tilde{\phi}$. In Eq.(71) we prescribe the function $< \hat{\Sigma}(x,y) >_y$ and show that the numerical solution agrees with the analytic result. Similarly, in Eq.(72), we neglect the Σ terms and verify that the linearized Eq. (72) simply propagates the solution in the y direction at a velocity given by

$$V_y = \frac{\omega}{k_y} = V_0 + \frac{\alpha + \hat{\rho}^2\bar{\phi}_{xxx}}{1 + \hat{\rho}^2 k_0^2}. \tag{73}$$

The next important test was to make sure that at early times, the code results agreed with the 'four-wave' linear theory when the pump wave amplitude was kept fixed. We did this by plotting the logarithm of the amplitude of the averaged potential $(\bar{\phi})$ against time and evaluating the slope. Since we were testing for accuracy, it was important that we compare the growth rates obtained from the code to the exact expression for the growth rate as given by Eq. (45). Rewriting the imaginary part of Eq. (45) in terms of the dimensionless parameters, we have the expression

$$\gamma = k_y \alpha q^2 \hat{\rho} G(\mathbf{k}, q) \left[2 \left(\frac{A_0}{\alpha q \hat{\rho}^2} \right)^2 \frac{(1 + (k_0^2 - q^2)\hat{\rho}^2)(1 + k_0^2\hat{\rho}^2)}{G(\mathbf{k}, q)} - 1 \right]^{1/2}, \tag{74}$$

where

$$G(\mathbf{k}, q) = \frac{1 + \hat{\rho}^2(k_y^2 + q^2 - 3k_x^2)}{(1 + \hat{\rho}^2 k_+^2)(1 + \hat{\rho}^2 k_-^2)(1 + \hat{\rho}^2 k_0^2)}.$$

We can simplify this relation by taking the usual zonal flow condition that the sidebands have a radial wave vector just slightly shifted from the pump wave i.e. $q \ll k_x, k_y$. This

allows us to write $G(\mathbf{k}, q) \approx (1 + \hat{\rho}^2(k_y^2 - 3k_x^2))/(1 + k_0^2\hat{\rho}^2)^3$. Therefore in the limit of small q, Eq. (74) reduces to

$$\gamma = \sqrt{2}|k_y q||A_0| \left(\frac{1 + (k_y^2 - 3k_x^2)\hat{\rho}^2}{(1 + k_0^2\hat{\rho}^2)} \right)^{1/2}. \tag{75}$$

In order to compare our results with earlier work[6, 22], it is important to compare the *reduced growth rate* γ/ω_0. This quantity is independent of the normalization conventions involving c_s, ρ_s etc. Upon evaluation, we find that our expressions agree exactly with the earlier results. Shown in Figure 1 are plots of the growth rates from the code (denoted by the line marked with circles) plotted with the growth rates from Eq. (74) (unmarked line) and Eq. (75) (line marked with squares) as a function of $\hat{\rho}$, A_0, m_x, m_y where $m_{x,y} = k_{x,y}/2\pi$. The agreement between the numerical results and Eq. (74) is excellent (within a few percent for all cases), but more importantly, the simplified dispersion relation from Eq. (75) shows good qualitative agreement, and only minor quantitative differences.

In the nonlinear evolution problem, a key test is to verify the conservation properties. We first consider the behaviour of the 'four-wave' invariants, I_0, I_B (cf. Eqs. (69,70)). It is clear that since the exact equations involve many interactions neglected in the four-wave theory, these quantities are not expected to be true invariants (unlike I, J derived in Section 2). Rather, their invariance over a certain epoch denotes the time interval over which the four-wave theory can be expected to provide a reasonable description of the system dynamics. On the other hand, a very sensitive check on the 'faithfulness' of the numerics is provided by the degree of accuracy and length of time over which the exact invariants, I, J are demonstrably maintained constant in the numerical solution of the nonlinear equations of motion.

Shown in Figure 2 is the time evolution of the amplitudes $|A_0|^2$ (line with the circles), $|a_+|^2$ (denoted by the squares), $|a_-|^2$ (denoted by the triangles), and the four-wave invariant I_0 (denoted by the bold solid line) for the parameters $\alpha = 1$, $\hat{\rho} = 0.01$, $A_0 = 0.001$, $m_x = m_y = 4$, and $m_q = q/2\pi = 2$. Also plotted on this graph is the enstrophy integral I which is denoted by the line with the solid cicles. Note that I quite clearly remains constant over the entire period of the simulation. The growth time for this case is about t = 3.3 in our normalized units. In contrast to I, the quantity I_0 remains constant for about 3 growth times, while the mode intensities ('energies') depart markedly from their initial values. It follows that beyond this time, many other modes become significant so that the four wave description of the system

loses its validity. The important point, however, is that the quantity I_0 keeps its value even after the pump wave has transferred about half of its energy to the sidebands. So clearly, I_0 can be considered to be a constant of the system so long as the four-wave model remains valid. It should be noted that although I_0 only remains constant over about 3 growth times, the more important time scale here is drift period of the pump wave, $\tau_d \sim 1/\omega_0$. If we compare the drift frequency $\omega_0 \sim k_y V_D$ to the growth rate, which from Eq. (75) scales as $\gamma \sim k_y q \rho_s c_s A_0$, we find that $\omega_0/\gamma \sim 1/(qL_n A_0)$, which for a small pump wave amplitude is much greater than unity. Therefore, the quantity I_0 remains a constant for hundreds of drift times. We find a similar behavior for the second four-wave invariant, I_B. Shown in Figure 3 is the time evolution of $|B|^2$ (denoted by the circles), $|a_+|^2$ (denoted by the squares), $|a_-|^2$ (denoted by the triangles), I_B (denoted by the bold solid line), and the energy integral J (line with solid circles) for the same parameters as for Figure 2. As was the case for I_0, the quantity I_B remains constant while the other quantities show significant growth for about three growth times when the four-wave model ceases to be valid due to generation of other modes. As expected, the integral invariant J remains constant for as long as the simulation was continued, showing that our numerical scheme 'faithfully' conserves the exact integrals of motion of the system over many linear growth times, thereby providing an excellent check on the numerical scheme employed.

We next address the issue of how this system behaves nonlinearly. For the runs, we choose parameters typical of a tokamak edge plasma; $L_N \sim 2-5$ cm, $\rho_s \sim 0.5-1$ cm, which, for a box size ($a = L_y$) of 10 cm gives us $\hat{\rho} = 0.005 - 0.01$ and $\alpha = 2-5$. Therefore, unless otherwise stated, the basic values of the parameters that we shall use will be $\hat{\rho} = 0.0075$, $\alpha = 3$, $m_x = m_y = 4$, and $A_0 = 0.01$. As a starting point, we shall discuss the nonlinear evolution of this case.

Shown in Figure 4 is a plot of $\bar{\phi}$ vs. x at a late nonlinear time. Clearly the averaged potential has a pronounced $m_q = 10$ structure, and since $\mathbf{V}_0 \sim m_q \bar{\phi}$, this suggests that the averaged flow will be dominated by the $m_q = 10$ mode. It is of interest to note that using the formula, Eq.(23), we find that the estimated value of the number of effective degrees of freedom of the system for the chosen conditions to be, $N_{\text{eff}} \simeq 10 - 15$. Thus the numerical evidence is in agreement with the theoretical estimate based on the exact invariants. The simulations show that this is a case of a zonal flow varying on 'radial' spatial scales comparable to or more rapidly than the pump wave. In order to get a better feel for the actual evolution of the mode structure, Figure 5 (a) shows the

time dependence of the $m_q = 1 - 5$ Fourier components of $\bar{\phi}$, and Figure 5 (b) the time dependence of the $m_q = 6 - 10$ modes. It is clear from these plots that since the $m_q = 1$ and $m_q = 2$ modes (denoted by the two boldest lines respectively) saturate at an amplitude comparable to the $m_q = 10$ mode (denoted by the line with circles), the zonal flow ($V_0 \simeq m_q \bar{\phi}$) will be dominated by the $m_q = 10$ mode, confirming the above conjecture.

The reason for this can be understood if we examine the dependence of the growth rate given by Eq. (75) upon m_q. Plotted in Figure 6 is γ as a function of m_q for $\alpha = 1, 3, 5, 7, 9$. For $\alpha = 3$ (the value corresponding to Figs.4 and 5a,b), the growth rate peaks at about $m_q \sim 10$, while for increasing α (which corresponds physically to a shorter L_n), the peak of the growth rate shifts to lower m_q. This can be seen from the approximate dispersion relation which is given in Eq.(48), which also demonstrates that the shorter wavelengths stabilize for large α. The question then arises as to whether a zonal flow does form for larger α.

Shown in Figure 7(a) is a plot similar to Figure 4, except that we now have, $\alpha = 7$. The averaged potential for this case has a decided sawtooth-like structure, which indicates that the averaged $\mathbf{E} \times \mathbf{B}$ flow will be a highly localized, jet-like structure (cf. [12],[26]) with a weaker reverse zonal flow away from this region. Recalling that the Fourier series of a sawtooth wave is given by

$$\bar{\phi}(x) \sim \sum_{m=1}^{m_{max}} \sin(2\pi m x)/m,$$

we can gain understanding as to why such a structure will form if we refer back to Eq. (72). In steady state, we can neglect the time derivative, and also neglect the term $\hat{\Sigma}$, as it is nonlinear in $\tilde{\phi}$, and can be neglected for small pump wave amplitude. The equation now reads,

$$\frac{\partial \tilde{\phi}}{\partial y}\frac{\partial \bar{\phi}}{\partial x}(1 + k_\perp^2 \rho_s^2) + \alpha \frac{\partial \tilde{\phi}}{\partial y} + \hat{\rho}^2 \frac{\partial \tilde{\phi}}{\partial y}\frac{\partial \bar{\phi}_{xx}}{\partial x} = 0, \tag{76}$$

which if we take $\partial/\partial x \sim iq$, leaves us with the algebraic relation,

$$\tilde{\phi} \sim \frac{i\alpha}{q} \frac{1}{(1 + (k_\perp^2 - q^2)\rho_s^2)}. \tag{77}$$

This qualitative argument suggests that the averaged potential tends to saturate so that the amplitude of each harmonic depends upon the reciprocal of the harmonic number, resulting in a 'sawtooth' wave form.

Another interesting feature of the saturation amplitudes that we observed from the simulations is that if α gets too large, then the amplitude of the saturated averaged potential drops dramatically. Shown in Figure 7(b) is a plot of $\bar{\phi}(x)$ for $\alpha = 9$. The potential is still sawtooth-like (although not as dramatic as for $\alpha = 7$), however, the saturated amplitude of the averaged potential is nearly an order of magnitude smaller. This may be due to the fact that for such α's, the longest wavelength mode which can be 'fitted' into the box falls outside the unstable range of wave lengths.

As a final example of how the modes vary in time, shown in Figure 8 are plots of the Fourier spectrum of $\bar{\phi}$ at early [Fig. 8(a)] and late [Fig. 8(b)] times and a surface plot of the Fourier spectrum of $\tilde{\phi}$ in k_x and k_y space at early [Fig. 8(c)] and late [Fig. 8(d)] times. The parameters used for this run were $\alpha = 5$, $\hat{\rho} = 0.002$, $A_0 = 0.001$, $m_x = 4$ and $m_y = 3$. At early times, the four wave description is quite apparent, with only the $m_q = 1$ mode in the spectrum of $\bar{\phi}$, and $\tilde{\phi}$ is quite obviously dominated by the pump wave. The two side bands are visible in the graph as well. At later time, the averaged potential has developed the $\bar{\phi}(k_x) \sim 1/k_x$ behaviour indicative of a sawtooth. From Fig. 8(d), it is quite obvious that the energy has been spread to many other radial modes in the system which shows why the higher order modes in the zonal flow are driven.

We have also varied the value of $\hat{\rho}$ and found results similar to those obtained when α was varied. Thus, for small $\hat{\rho}$ (< 0.01), the averaged potential was dominated by the fastest growing short wavelength modes. As $\hat{\rho}$ increased, however, the jet-like zonal flow occurred for lower values of α, for example, when $\hat{\rho} = 0.015$, a jet formed for $\alpha = 4$. This observation is consistent with the argument that in order for a zonal flow to form, the maximum growth rate must occur for low radial mode numbers, and as we showed earlier, $q_{max} \approx A_0/(\alpha\hat{\rho}^2)$. Likewise, when we varied the pump wave amplitude, we found a similar behaviour: thus, for A_0 very small (< 0.005), the jet formed for experimentally typical values of α and $\hat{\rho}$, while for larger A_0 (> 0.02), the averaged potential was dominated by the shorter wavelengths, and the jet only formed for unrealistically large values of α and $\hat{\rho}$.

6 Discussion and conclusions

The generalized Charney-Hasegawa-Mima model introduced by Smolyakov *et. al.* and others is clearly the simplest one which explicitly exhibits the modulational instability

mechanism of 'self-generated' zonal flows by drift waves. This mechanism itself has long been implicated in many problems in fluid mechanics and plasma physics. The discussion in Section 2 shows that through the medium of the 'side-bands', a zonal flow (ie a purely 'radial' electric field perturbation with zero linear frequency) is able to extract energy from a typical drift wave ('pump'), provided some rather mild threshold conditions are met. What is interesting about this dissipationless system is that, at least for a few initial growth times, the pump is 'drained' of energy by the growing zonal flow and the drift wave side-bands. This is the start of a typical 'inverse cascade' process which is known to play a fundamental role in much more elaborate tokamak simulations[12]. In effect, 'pump draining' by the growing zonal flow and the side-bands provides a nonlinear saturation mechanism for drift modes driven unstable by some unspecified source. The energy of the pump drift wave is thereby distributed over a much wider spectrum of drift wave frequencies through the mediation of the zonal flow. Although this is a typical 'profile-turbulence interaction', it is distinct from more usual 'quasi-linear' saturation mechanisms which rely on the turbulence-generated transport *modifying* the equilibrium gradients which drive the linear modes, and those in which the sheared zonal flow directly 'decorrelates' the turbulent fluctuations radially by breaking up turbulent eddies.

During the *nonlinear* phase of the four-wave interaction between a specific 'pump wave', its side-bands and an associated zonal flow, it is remarkable that two 'invariants', I_0, I_B exist for many drift periods. However, due to the eventual nonlinear generation of other modes permitted by the threshold conditions (but not initially present), the four-wave model loses its validity. This happens because the system is not well-described by four coupled modes since other four-wave groups can also occur. These can all interact with each other in the fully nonlinear stage. The full system however was shown to have two positive definite invariants which permit the following deductions: the linear growth of the zonal flow *must* be saturated eventually; the total number of new 'modes' generated nonlinearly cannot increase indefinitely, but is in fact determined by the initial conditions (via the values of I, J at $t = 0$). In the long run, the system motion must be 'recurrent'[23, 24]. The last statement implies that the pump must eventually reconstruct itself, although under practically relevant conditions, the recurrence times may be too long to be of interest. This type of 'cyclic' relaxation behaviour of zonal flows and turbulence, is, in the present simple model, a consequence of energy and enstrophy conservation. However, it is remarkable that in driven, dissipative systems such

as those considered in more elaborate simulations of tokamak turbulence (eg. Ref.[12]) very similar behaviour is found, suggesting that the conservative model captures in some sense the essence of the phenomenon of continual cyclical relaxational exchange of energy and enstrophy between zonal flows and plasma turbulence(the losses being compensated by the external drives) in more realistic systems.

The numerical simulations presented in Section 5 demonstrate the following noteworthy features. The linear phase of the four-wave model accurately represents the initial system behaviour. The four-wave nonlinear model, while not valid over more than a few linear growth times, nevertheless gives a good qualitative account of the 'stabilization' of the turbulence by the inverse cascading of energy into the zonal flow (of course the side-bands are also involved in this process). The four-wave 'invariants' (I_0, I_B) are good indicators of how long the reduced model remains valid. Unlike the 'wave kinetic' formalism [6] which does not represent the full nonlinearities inherent in the system, the exact invariants are clearly conserved in the present simulations over much longer time-scales. Furthermore, the estimated number of effective modes[23] is substantially in agreement with the predictions of the code. The full numerical simulations also show that not only can zonal flows develop 'corrugations' and/or 'jet-like' structures(cf. [12]), they can also be dramatically reduced in some conditions. These different structural forms appear to be controlled by the α parameter, the dimensionless Larmor radius parameter $\hat{\rho}$, and the initial data: i.e., the initial pump wave amplitude. In particular, the dramatic reduction of zonal flows (and consequent loss of a damping mechanism for the turbulence) when α exceeds a certain threshold, is suggestive of a possible route from H to L modes, although one must be cautious about drawing definitive conclusions from such a simplified two-dimensional model. What is clear is that the radial electric field structures obtained in [12] exhibit many of the features presented here. It is of interest to note that the present model exemplifies systems where the zonal flows are *entirely* generated by the turbulence without any assistance from neoclassical effects, and/or externally driven flows. In power plant conditions, it is probable that most of the zonal flows in the plasma could be of this type.

The dynamics of zonal flow-turbulence interactions studied here suggest the possible existence of much more general mechanisms which remain to be explored. Is there a corresponding 'inverse cascade' via modulational instabilities of short wave-length modes to the entire long wave-length (ie small k_x, k_y) spectrum? The existence of such a mechanism would serve to illuminate many features of the turbulence calculated by

'first-principles' codes, and may also explain why experimentally there never has been any conclusive observation of significant turbulence in the really 'high'($k_\perp \rho_s \geq 0.3, \frac{\omega}{2\pi} \simeq$ 1MHz) part of the spectrum. The questions of relationship between purely electrostatic, fluid-based, two-dimensional models like the present one and more realistic models have yet to be elucidated. The present investigation forms a basic starting point from which we hope to pursue these matters more systematically in the future.

Acknowledgements: The authors acknowledge useful discussions with Jack Connor, Colin Roach, Giovanni Manfredi and Richard Dendy. This research was jointly funded by the UK Dept. of Trade and Industry and Euratom. DRM would like to acknowledge support from the United States Department of Energy Grant No. DE-FG02-96ER54370, and Southeastern Louisiana University. DRM would also like to thank the UKAEA for their kind hospitality and Bert Lester for his assistance with the numerics.

References

[1] C. Gormezano, Plasma Phys. Control. Fusion **41**, B367 (1999)

[2] M.G. Bell *et. al.*, Plasma Phys. Control. Fusion, **41**, A719 (1999).

[3] E.J. Strait *et. al.*, Phys. Rev. Lett. **75**, 4417 (1995)

[4] K.H. Burrell, Science, **281**, 1816 (1998).

[5] A. Hasegawa and M. Wakatani, Phys. Rev. Letts. **59**, 1581 (1987).

[6] A.I. Smolyakov, P.H. Diamond and V.I. Shevchenko, Phys. Plasmas, **7**, 1349 (2000).

[7] K. Itoh, S-I. Itoh and A. Fukuyama, *Transport and Structural Formation in Plasmas*, Inst. of Phys., Bristol, (1999).

[8] P.N. Guzdar, R.G. Kleva and Liu Chen, Phys. Plasmas, **8**, 459 (2001)

[9] W. Horton and A. Hasegawa, Chaos, **4**, 227 (1994).

[10] T.S. Hahm, K.H. Burrell, Z. Lin, R. Nazikian and E.J. Synakowski, Plasma Phys. and Control. Fusion, **42** A205 (2000).

[11] Z. Lin, *et. al.*, Phys. Rev. Lett., **83**, 3645 (1999).

[12] A. Thyagaraja, Plasma Physics and Contol. Fusion, **42**, B255 (2000).

[13] X. Garbet and R.E. Waltz, Phys. Plasmas, **5**, 2836, (1998).

[14] A. Zeiler, J.F. Drake and B.N. Rogers, Phys. Rev. Letts., **84**, 99 (2000).

[15] T.B. Benjamin, Proc. Roy. Soc. A **299**, 59 (1967).

[16] G.B. Whitham, *Linear and Nonlinear Waves*, John Wiley, New York, 527 (1974).

[17] T.F. Volkov, Fizika Plasmy, **4**, Izd. Akad. Nauk, SSSR, Moscow, 98 (1958). English Translation: *Plasma Physics and the Problems of Controlled Thermonuclear Reactions*, 4, Pergamon Press, London, 114 (1960).

[18] P.K. Kaw, G. Schmidt and T. Wilcox, Phys. Fluids, **16**, 1522 (1973).

[19] J. Drake, P.K. Kaw, Y.C. Lee, G. Schmidt, C.S. Liu and M.N. Rosenbluth, Phys. Fluids, **17**, 778 (1974).

[20] C.N. Lashmore-Davies, Phys. Fluids, **19**, 587 (1976).

[21] C.N. Lashmore-Davies, A. Thyagaraja and R.A. Cairns, Physics of Plasmas, **4**, 3243 (1997)

[22] G. Manfredi, C.M. Roach and R.O. Dendy, To be published in Proc. EPS 2001 Conference, Madeira, Portugal (2001)

[23] A. Thyagaraja, Phys. Fluids, **24**, 1973, (1981)

[24] A. Thyagaraja, in *Nonlinear Waves*, Cambridge monographs on mechanics and applied mechanics, Ed. Lokenath Debnath, Cambridge Univ. Press, Camb. UK, Ch. 17, 308 (1993).

[25] P. N. Guzdar, J. F. Drake, D. R. McCarthy, A. B. Hassam, and C. S. Liu, Phys. Fluids B **5**, 3712 (1993).

[26] G.M. Staebler, Phys. Rev. Letts., **84**, 3610 (2000).

Figure Captions

1. A plot of the normalized growth rate as a function of a) $\hat{\rho}$, b) A_0, c) m_x, and d) m_y. The unmarked line denotes the theoretical growth rate as given by Eq. (71), the line marked with squares shows the approximate growth rate as given by Eq. (72), and the line marked with circles is the code result. The basic parameters for each run were $\hat{\rho} = 0.01$, $A_0 = 0.01$, $m_x = m_y = 4$, and $\alpha = 1.0$.

2. A plot of the first four-wave invariant I_0, the pump wave amplitude squared, the sideband amplitudes squared, and the enstrophy integral I as a function of time. All quantities have been divided by the initial value of $|A_0|^2$ so as to normalize the initial invariant to unity, and the enstrophy integral has been normalized so as to give it an initial value of 0.5. The dark solid line is I_0, the line with the circles is $|A_0|^2$, the line with the triangles is $|a_-|^2$, the line with the squares is $|a_+|^2$, and the line with solid circles is I. The parameters were $\hat{\rho} = 0.01$, $A_0 = 0.001$, $m_x = m_y = 4$, $m_q = 2$, and $\alpha = 1.0$.

3. A plot of the second four-wave invariant I_B, the averaged potential amplitude squared, the sideband amplitudes squared, and the energy integral J as a function of time. All quantities have been divided by the initial value of $|A_0|^2$, and the energy integral has been normalized so as to give it an initial value of 0.15. The dark solid line is I_B, the line with the circles is $|B|^2$, the line with the triangles is $|a_-|^2$, the line with the squares is $|a_+|^2$, and the line with solid circles is J. The parameters used are the same as those used for Figure 2.

4. The averaged potential ($\bar{\phi}$) as a function of x at a late nonlinear time. The parameters for this run were $\alpha = 3$, $\hat{\rho} = 0.0075$, $m_x = m_y = 4$, and $A_0 = 0.01$. The $m_q = 10$ structure is apparent.

5. The time evolution of the Fourier amplitudes of $\bar{\phi}$ as a function of time for the same system as in Figure 4. 5 (a) shows the $m_q = 1 - 5$ modes, which are denoted by the unmarked line, the line with inverted triangles, the line with triangles, the line with squares, and the line with circles respectively. 5(b) shows the $m_q = 6 - 10$ modes, which are denoted in the same way as the modes in 5(a). The $m_q = 10$ mode, dominates the zonal flow.

6. A plot of the growth rate as given by Eq. (71) as a function of m_q for $\alpha = 1, 3, 5, 7, 9$. The lines corresponding to each value of α are labeled in the figure.

7. A similar plot to Figure 4, except α has a value of 7 in (a) and $\alpha = 9$ in (b). The sawtooth structure is evident, and note the dramatic drop in the saturated amplitudes.

8. Fourier spectrum of $\bar{\phi}$ at (a) early and (b) late times, and the Fourier spectrum of $\tilde{\phi}$ at (c) early and (d) late times. Figs. (a) and (c) show clearly the four wave structure of the system at early times, and Figs. (b) and (d) show the sawtooth-like spectrum of the averaged potential and the excitation of higher modes by wave-wave coupling of the potential.

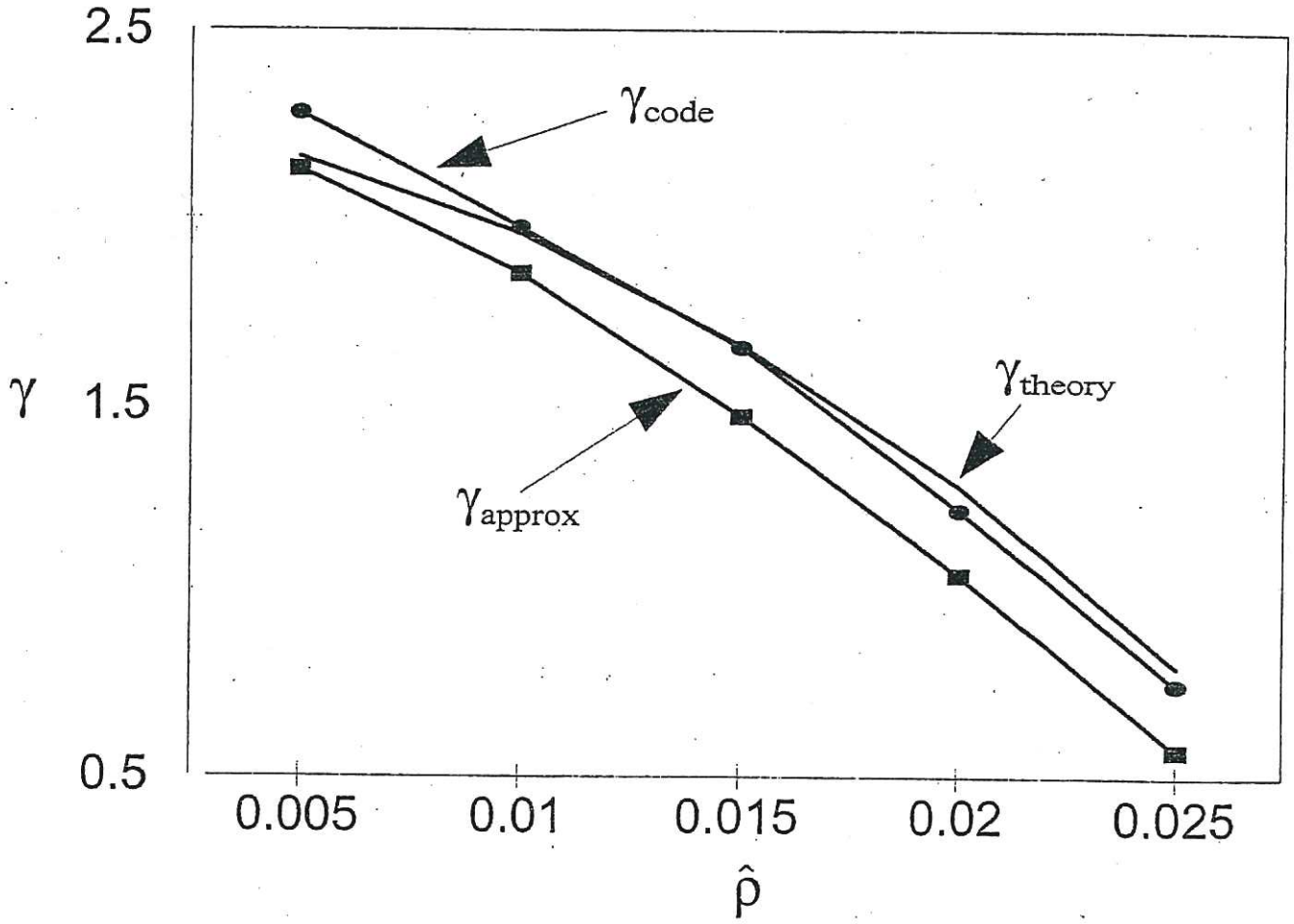

Figure 1 (a)

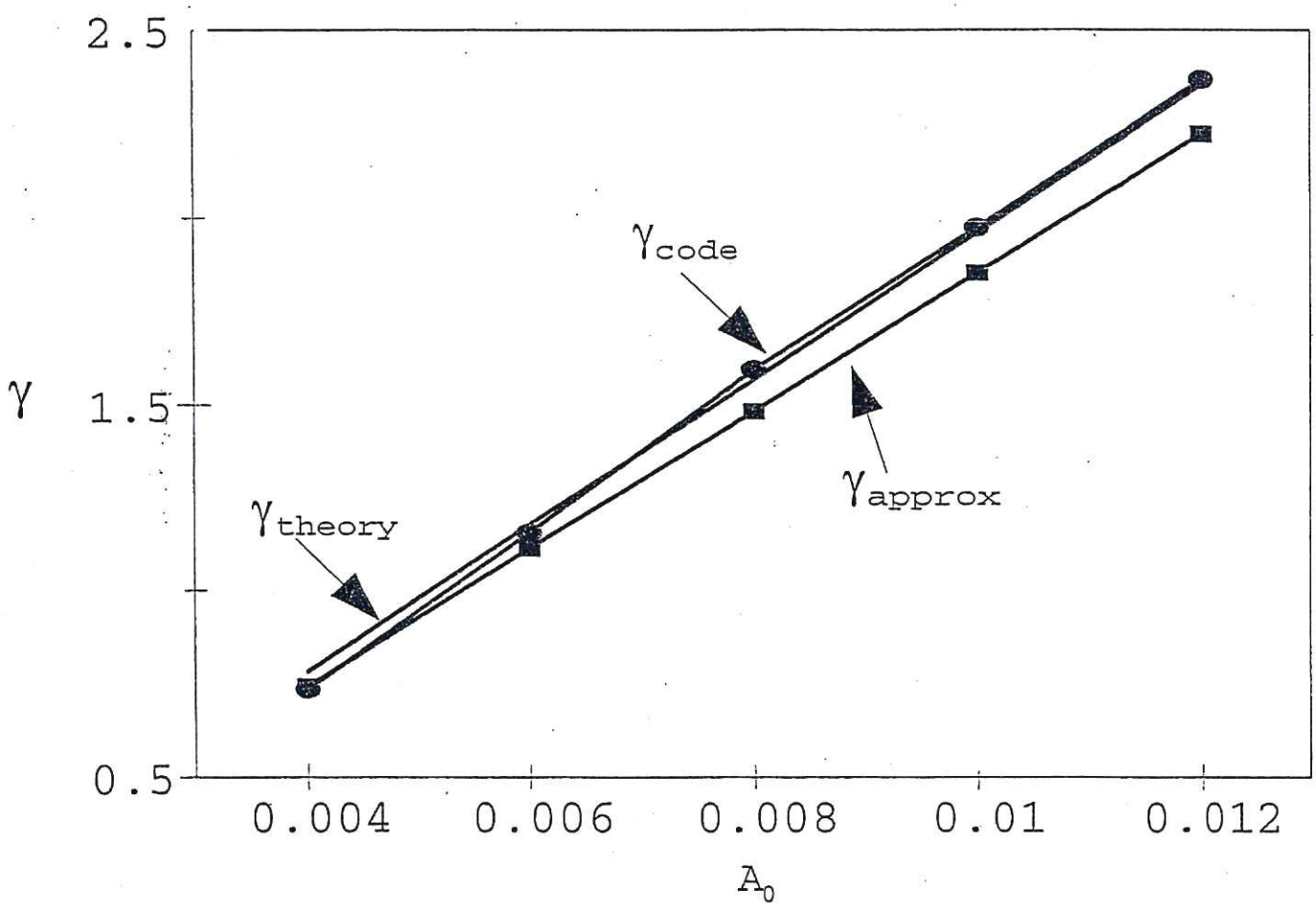

Figure 1(b)

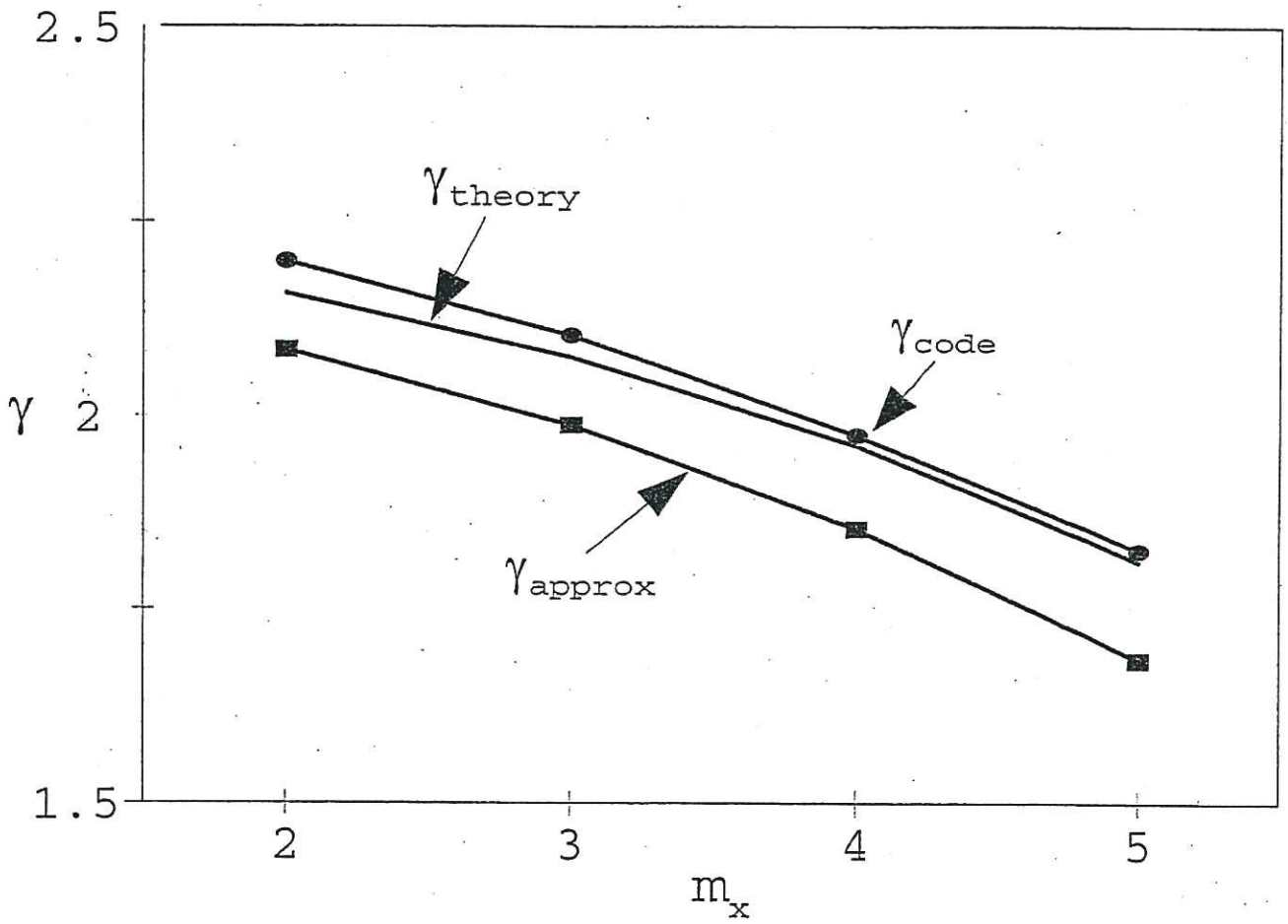

Figure 1(c)

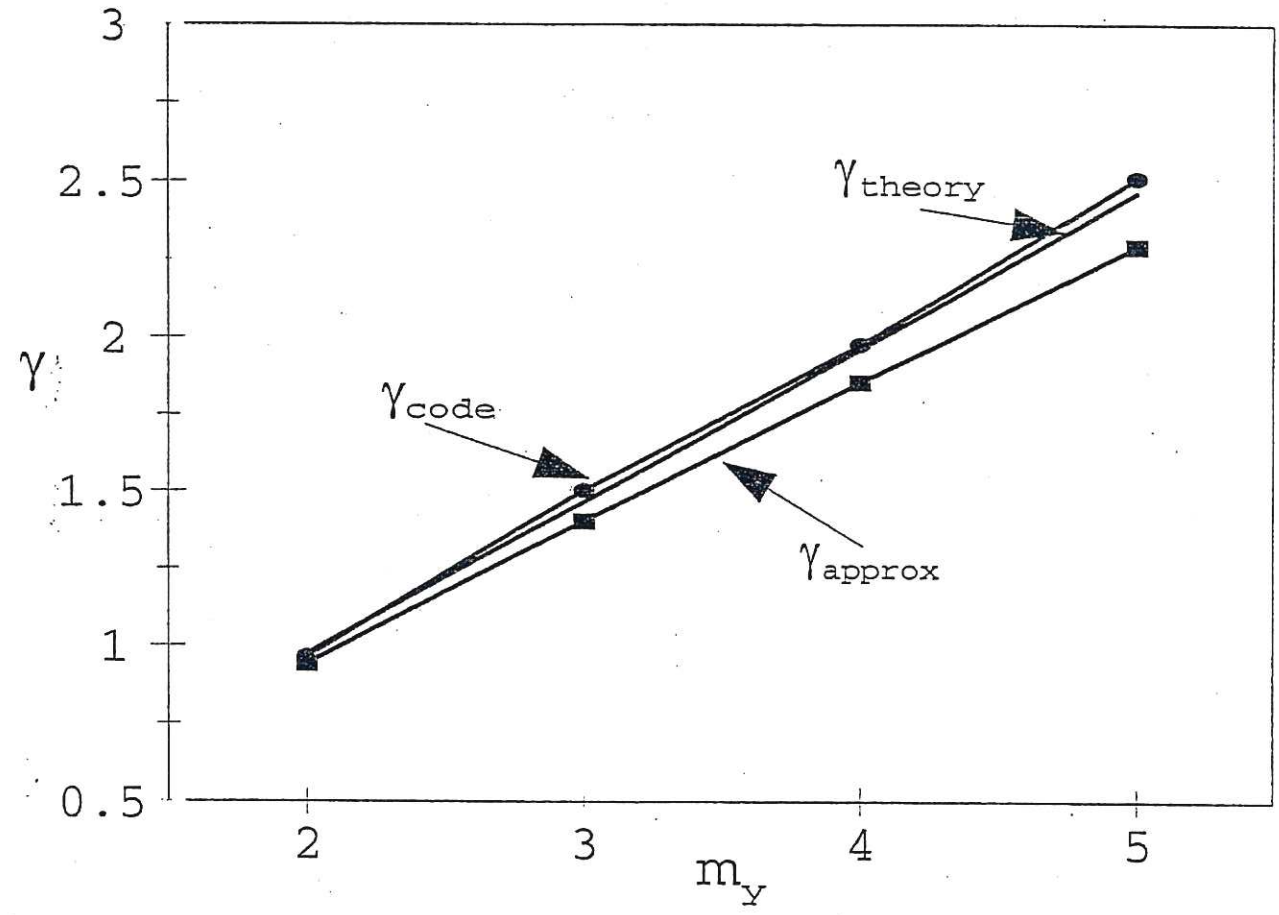

Figure 1(d)

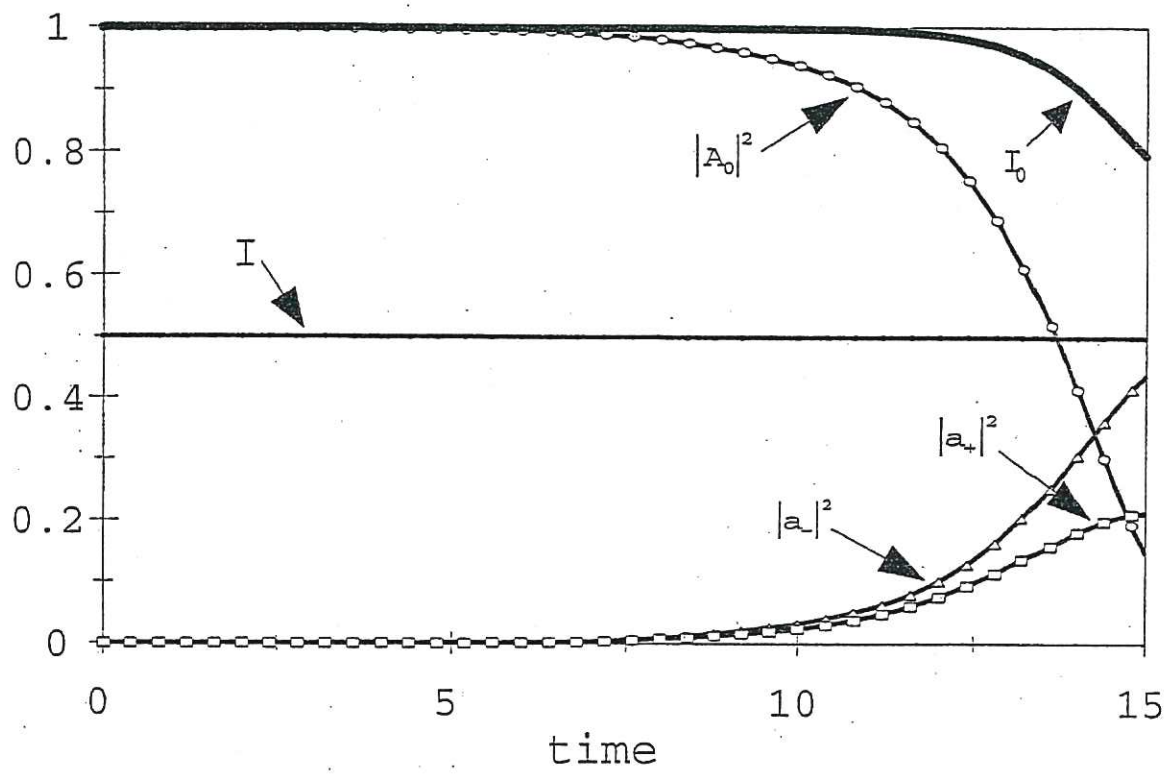

Figure 2

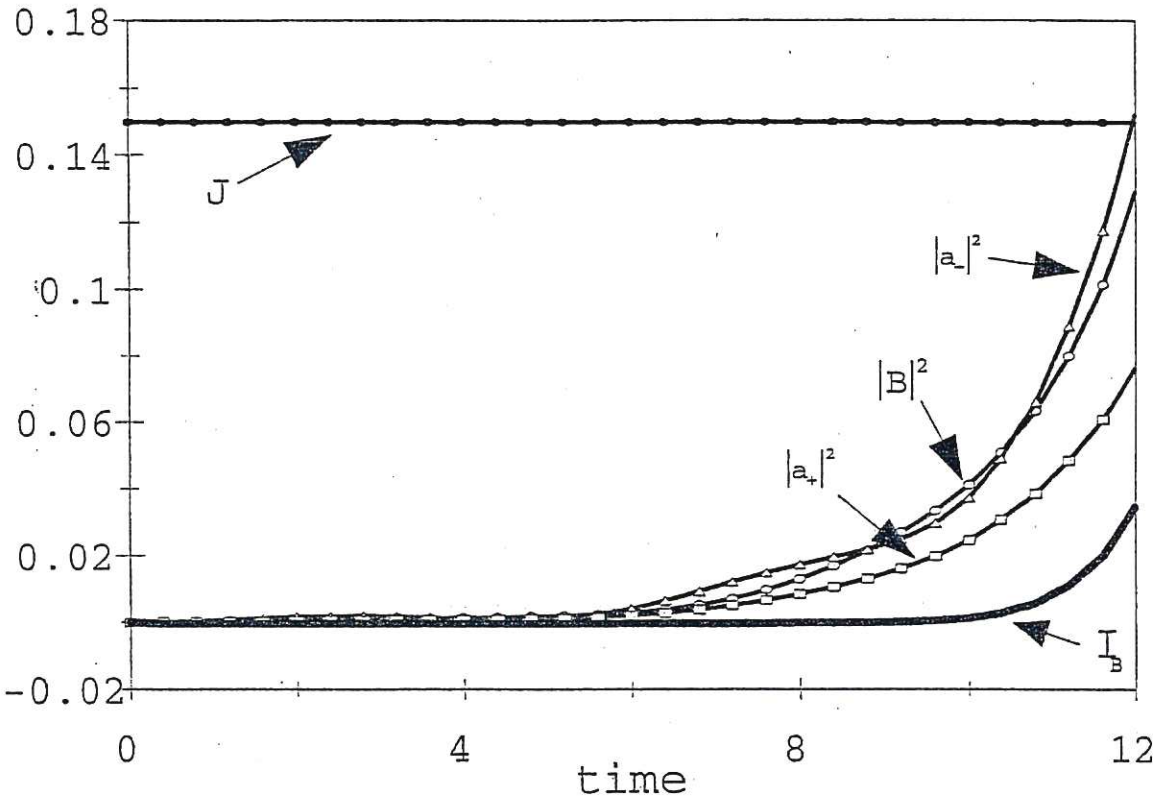

Figure 3

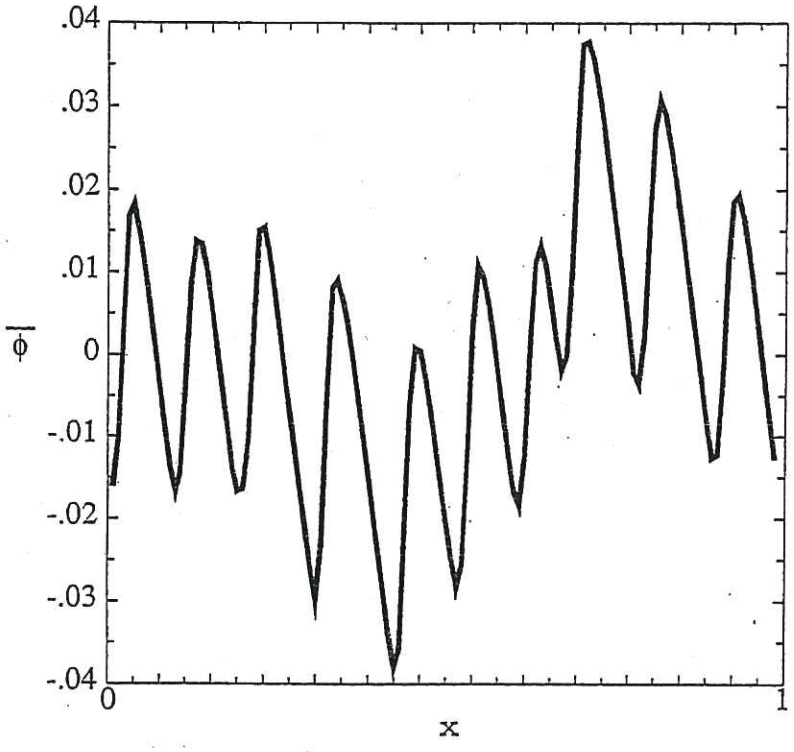

Figure 4

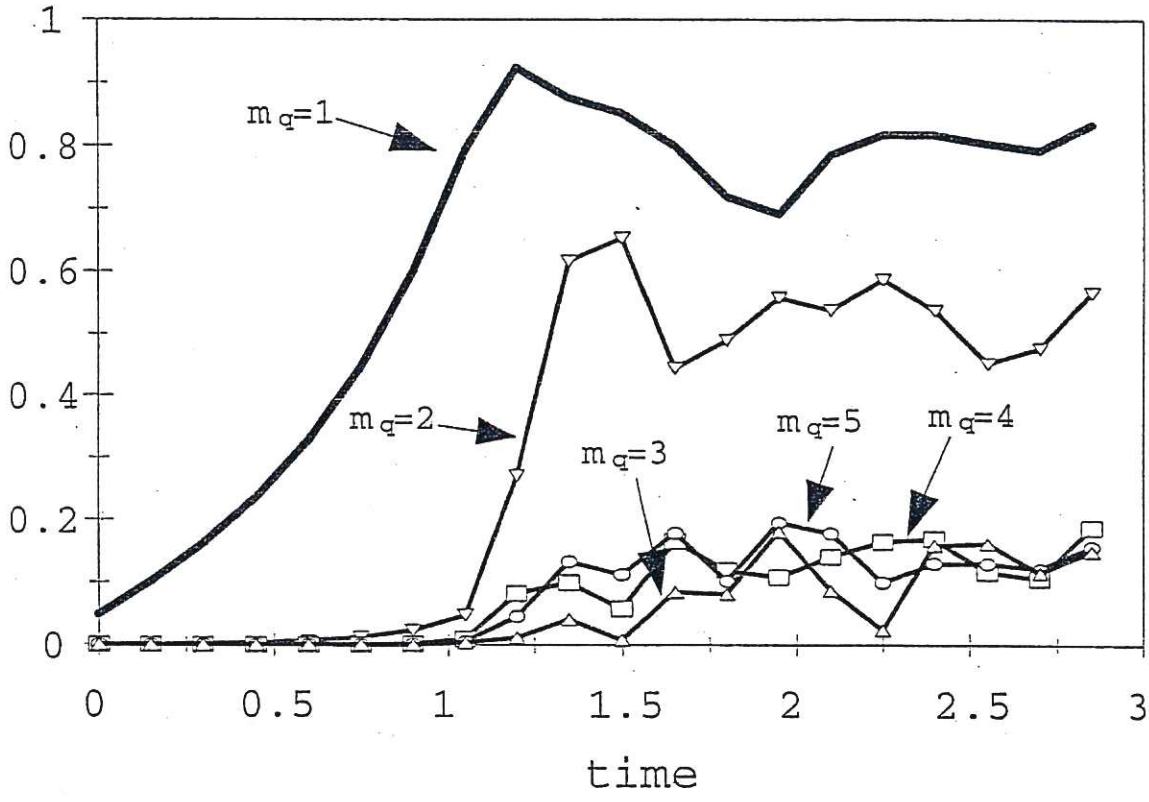

Figure 5(a)

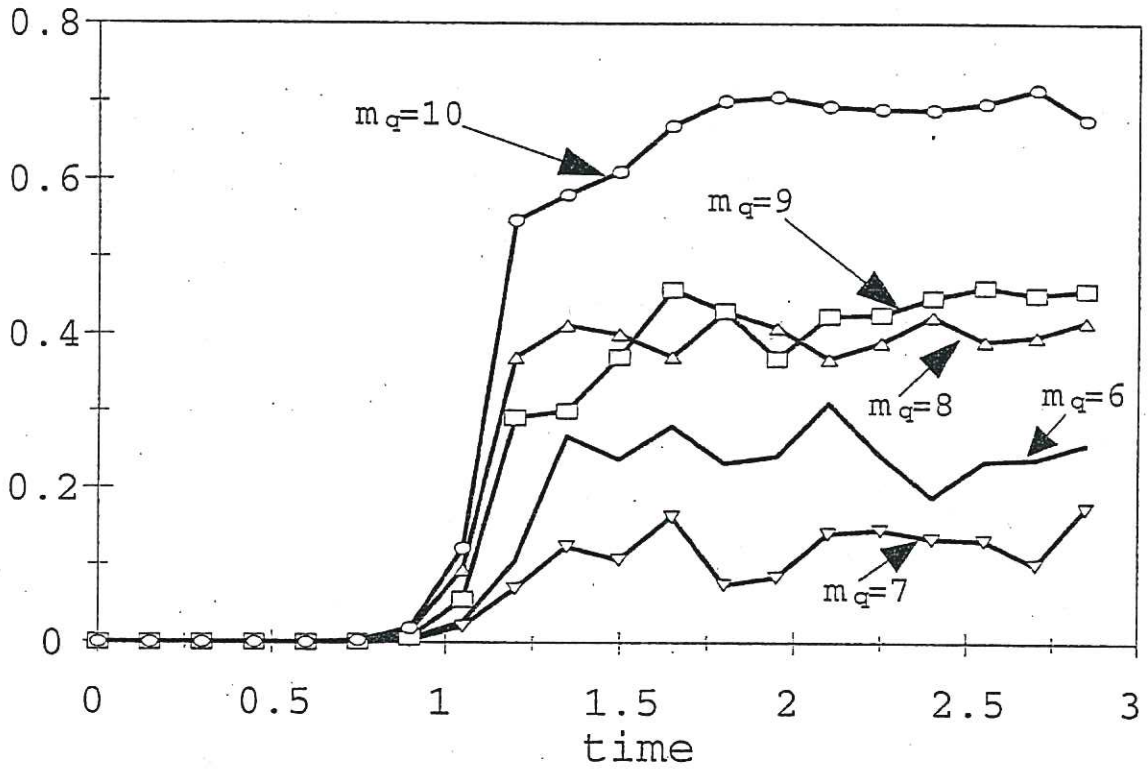

Figure 5(b)

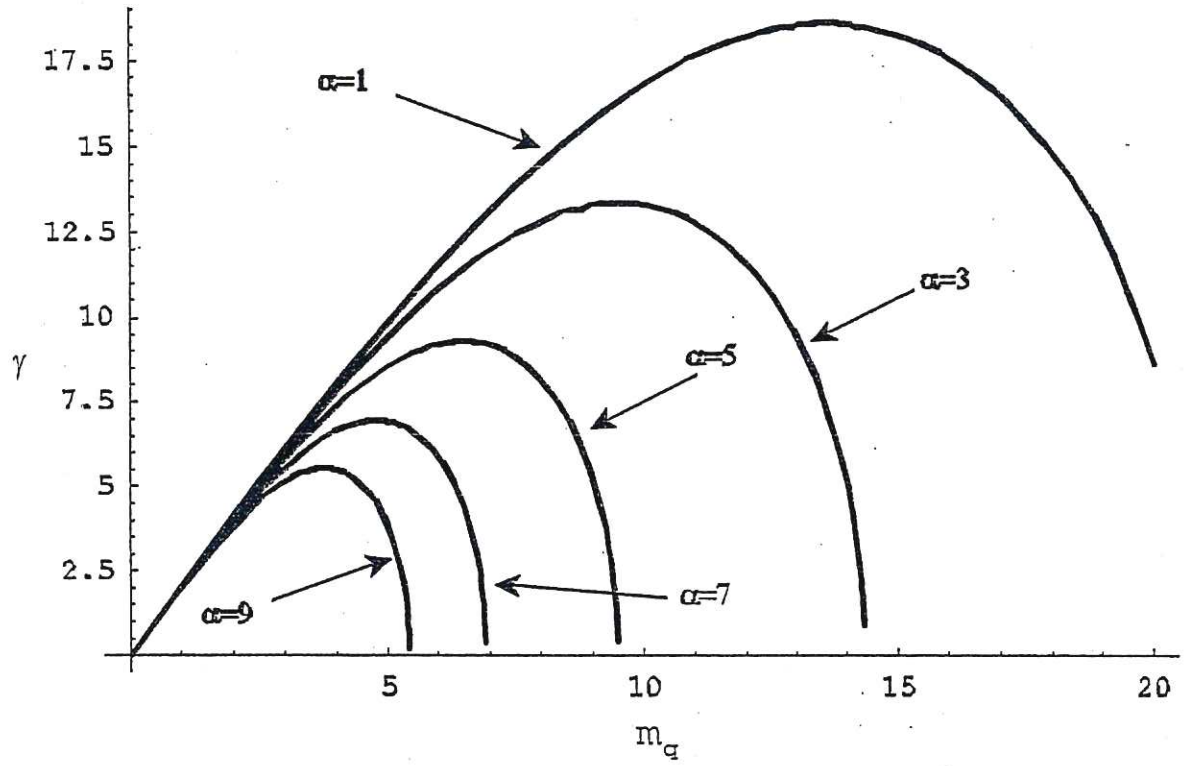

Figure 6

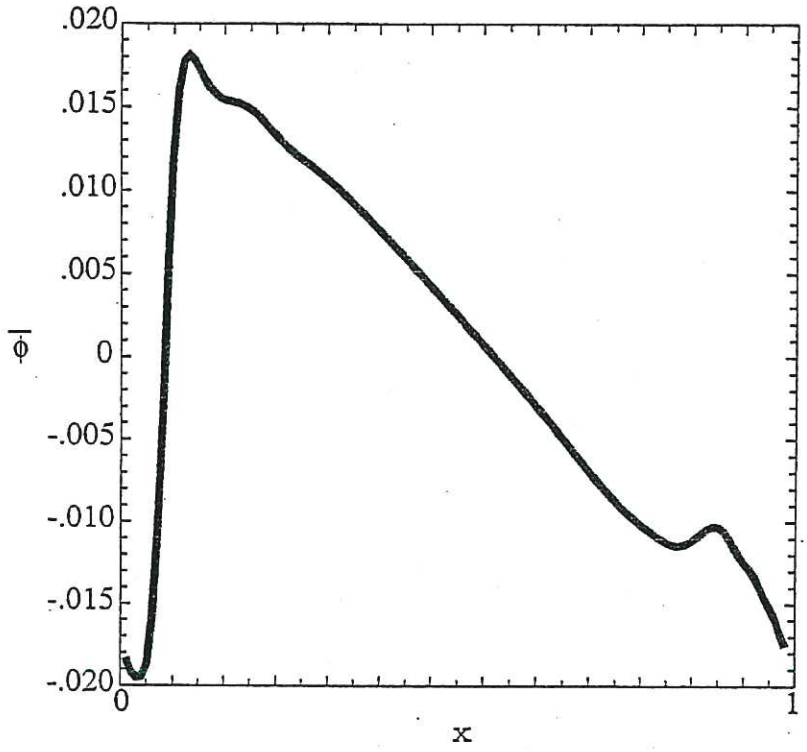

Figure 7(a)

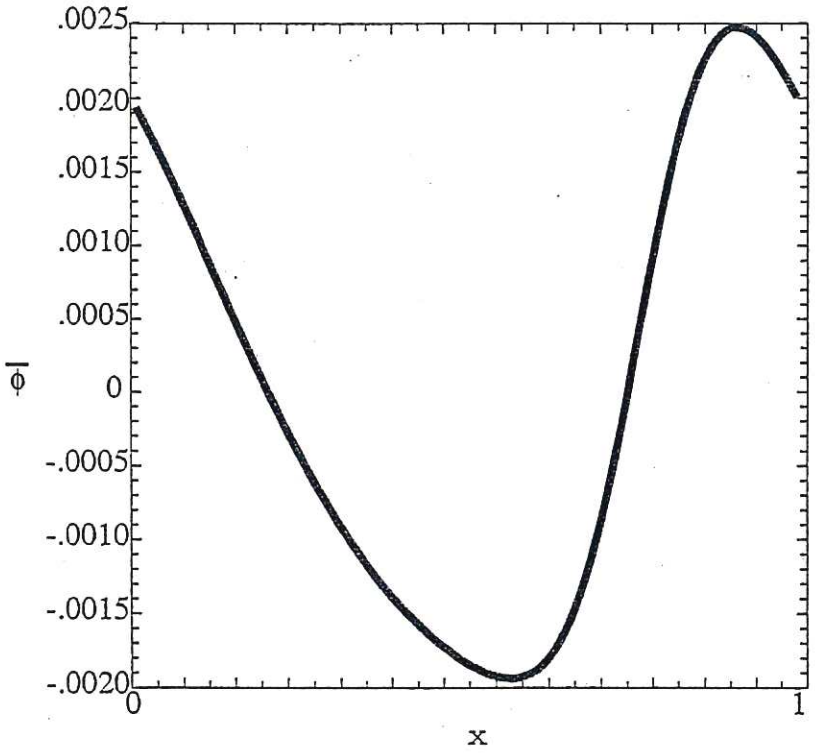

Figure 7(b)

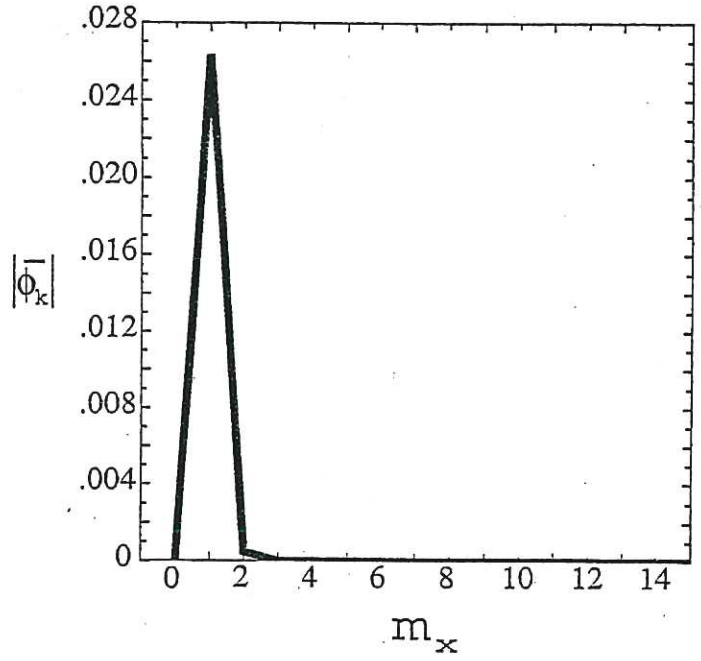

Figure 8(a)

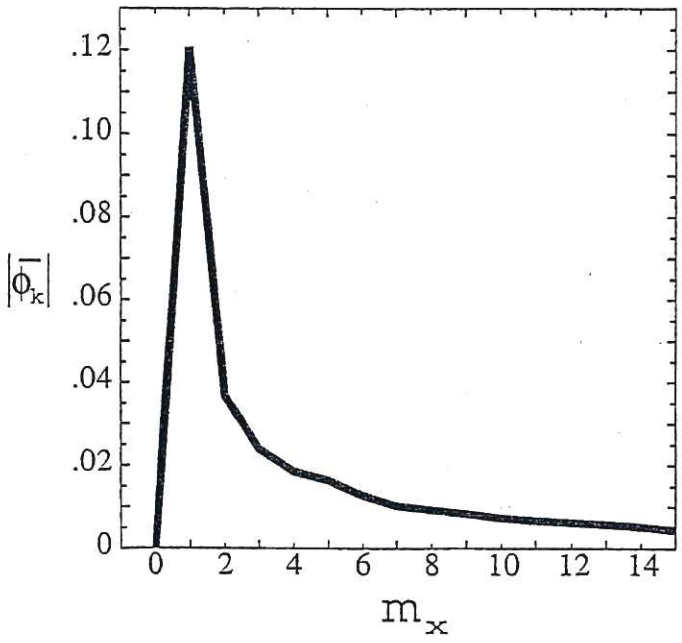

Figure 8(b)

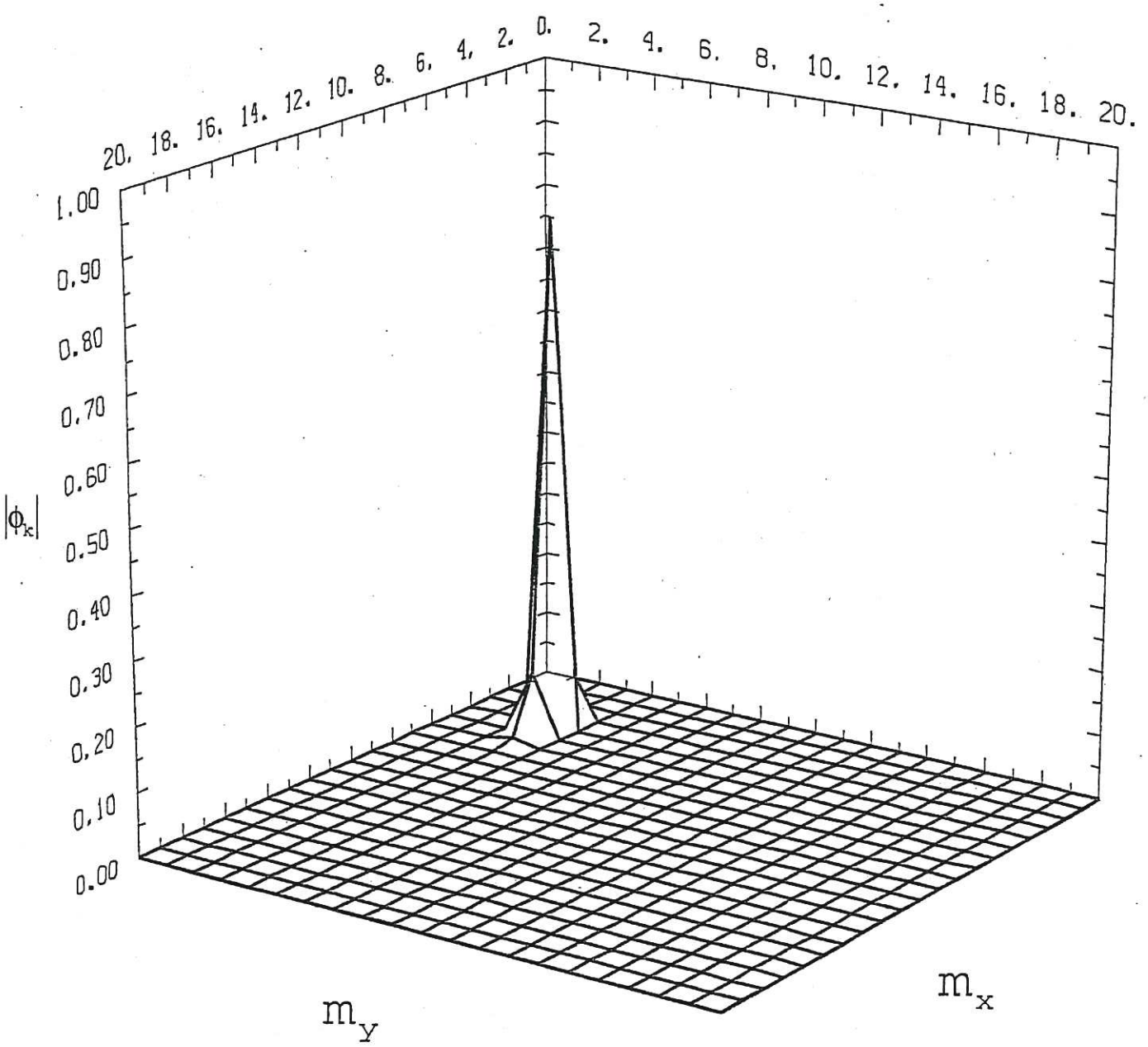
20. 18. 16. 14. 12. 10. 8. 6. 4. 2. 0. 2. 4. 6. 8. 10. 12. 14. 16. 18. 20.
1.00
0.90
0.80
0.70
0.60
0.50
0.40
0.30
0.20
0.10
0.00
$|\phi_k|$
m_y
m_x

Figure 8(c)

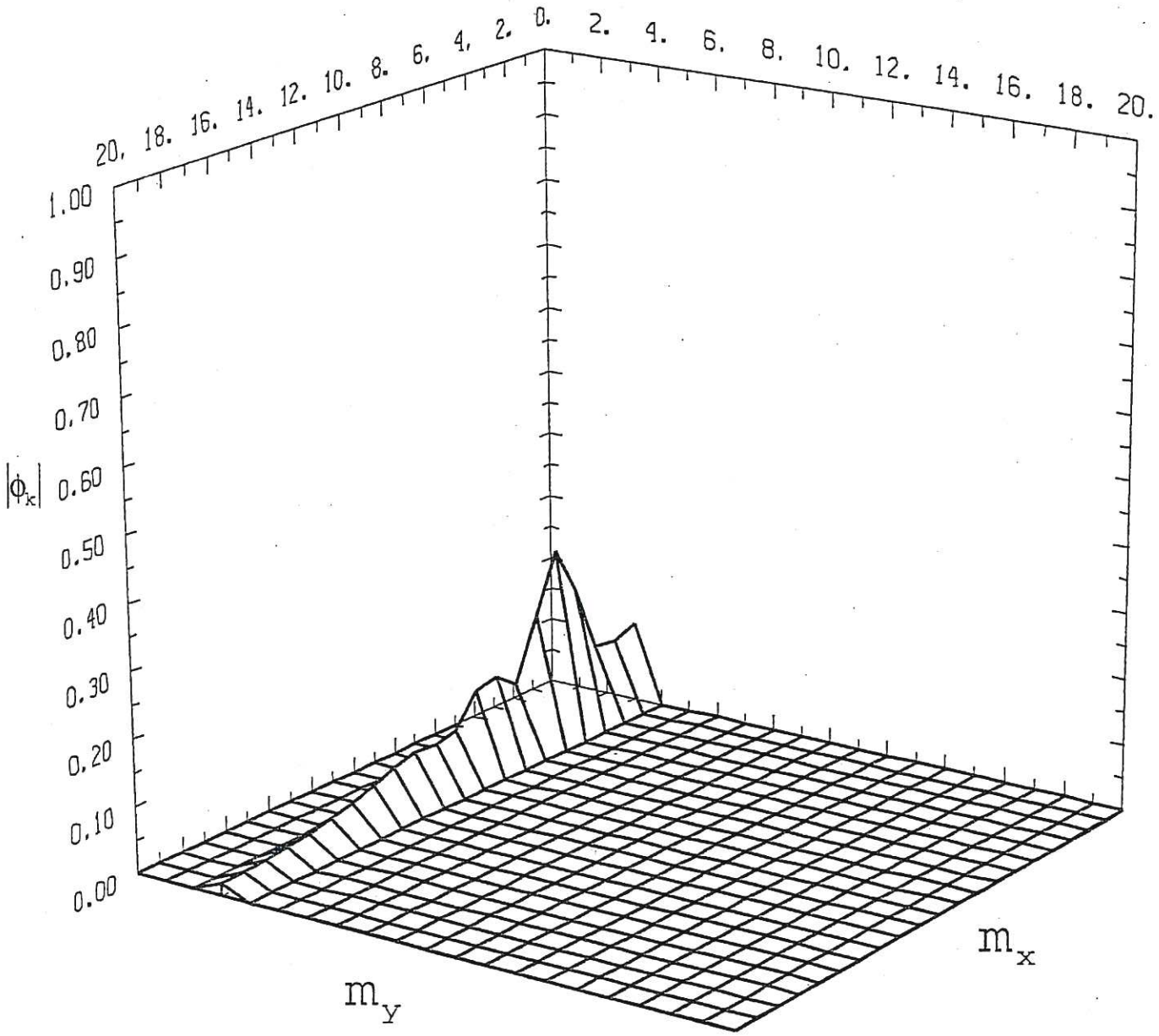
0. 2. 4. 6. 8. 10. 12. 14. 16. 18. 20.
20. 18. 16. 14. 12. 10. 8. 6. 4. 2.
1.00
0.90
0.80
0.70
0.60
0.50
0.40
0.30
0.20
0.10
0.00
$|\phi_k|$
m_y
m_x

Figure 8(d)